Seasonal evolution of net and regenerated silica production around a natural Fe-fertilized area in the Southern Ocean estimated from Si isotopic approaches

I. Closset[1], M. Lasbleiz[2], K. Leblanc[2], B. Quéguiner[2], A.-J. Cavagna[3], M. Elskens[3], J. Navez[4], D. Cardinal[1,4]

[1] {Sorbonne Universités (UPMC, Univ Paris 06)-CNRS-IRD-MNHN, LOCEAN Laboratory, 4 place Jussieu, F-75005 Paris, France}

[2] {Aix Marseille Université, CNRS, Université de Toulon, IRD, MIO UM 110, 13288, Marseille, France}

[3] {Earth and System Sciences & Analytical and Environmental Chemistry, Vrije Universiteit Brussel, Pleinlaan 2, B-1050 Brussels, Belgium}

[4] {Department of Earth Sciences, Royal Museum for Central Africa, Leuvensesteenweg 13, 3080 Tervuren, Belgium}

Correspondence to: I. Closset (ivia.closset@locean-ipsl.upmc.fr)

Abstract

A massive diatom-bloom is observed each year in the surface waters of the naturally Fe fertilized Kerguelen Plateau (Southern Ocean). We measured biogenic silica production and dissolution fluxes (ρSi and ρDiss respectively) in the mixed layer in the vicinity of the Kerguelen Plateau during austral spring 2011 (KEOPS-2 cruise). We compare results from a High-Nutrient Low-Chlorophyll reference station and stations with different degrees of iron enrichment and bloom conditions. Above the Plateau biogenic ρSi are among the highest reported so far in the Southern Ocean (up to 47.9 mmol m^{-2} d^{-1}). Although significant (10.2 mmol m^{-2} d^{-1} in average), ρDiss were generally much lower than production rates. Uptake ratios (ρSi:ρC and ρSi:ρN) confirm that diatoms strongly dominate the primary production in

28   this area. At the bloom onset, decreasing dissolution to production ratios (D:P) indicate that

29   the remineralization of silica could sustained most of the low silicon uptake and that the

30   system progressively shifts toward a silica production regime which must be mainly

31   supported by new source of silicic acid. Moreover, by comparing results from the two

32   KEOPS-expeditions (spring 2011 and summer 2005), we suggest that there is a seasonal

33   evolution on the processes decoupling Si and N cycles in the area. Indeed, the consumption of

34   H_4SiO_4 standing stocks occurs only during the growing stage of the bloom when strong net

35   silica production is observed, contributing to a higher H_4SiO_4 depletion relative to NO_3^-.

36   Then, the decoupling between H_4SiO_4 and NO_3^- is mainly controlled by the more efficient

37   nitrogen recycling relative to Si. Gross-Si:N uptake ratios were higher in the Fe-rich regions

38   compared to the HNLC area, likely due to different diatoms communities. This suggests that

39   the diatom responses to natural Fe fertilization are more complex than previously thought, and

40   that natural iron fertilization over long time scales does not necessarily decrease Si:N uptake

41   ratios as suggested by the Silicic Acid Leakage Hypothesis. Finally, we propose the first

42   seasonal estimate of Si-biogeochemical budget above the Kerguelen Plateau based on direct

43   measurements. This study points out that naturally iron fertilized areas of the Southern Ocean

44   could sustain very high regimes of biogenic silica production, similar to those observed in

45   highly productive upwelling systems.

46

47   **1   Introduction**

48   Covering 20 % of the World Ocean, the Southern Ocean is considered as a crucial component

49   of the climate system since it represents a net sink for atmospheric CO_2 (Takahashi et al.,

50   2009). It also plays a key role in the global silicon (Si) biogeochemical cycle because diatoms,

51   a siliceous phytoplankton group, are one of the major primary producers in this area

52   (Buesseler et al., 2001; Quéguiner and Brzezinski, 2002; Tréguer and De la Rocha, 2013). As

53   their cell wall is composed of biogenic silica (opal, amorphous $SiO_2.nH_2O$, hereafter referred

54   to as BSi), diatoms take up dissolved silicon (hereafter referred to as DSi) in the form of

55   silicic acid (H_4SiO_4), to produce their siliceous frustules. At global scale, 56 % of this gross

56   production is estimated to be directly recycled in the upper 100 m (Tréguer and De La Rocha,

57   2013) due to the combined effects of both physico-chemical and biological processes

58   (Kamatani, 1982; Bidle and Azam, 1999; Ragueneau et al., 2000). Only the material escaping

59   dissolution is exported toward the deep ocean and eventually buried in sediments.

60   Consequently, the marine Si biogeochemical cycle is dominated by biogenic silica production

61   and dissolution in the surface mixed layer, and one atom of Si undergoes a cycle of biological

62   uptake by diatom and subsequent dissolution about 25 times before being removed to the

63   seabed (Tréguer and De La Rocha, 2013). Thus, it is essential to estimate the balance between

64   silica production and dissolution in the euphotic zone which is best illustrated by the

65   integrated dissolution to production rate ratio ($\int$D:$\int$P; Brzezinski et al., 2003) or by integrated

66   net production rate ($\int\rho$Si$_{Net}$ = production minus dissolution). Globally, the $\int$D:$\int$P values present

67   an annual mean of 0.56 (Tréguer and De La Rocha, 2013) and range from < 0.1 to > 1, with

68   low D:P values associated to diatom bloom events, and D:P values exceeding 0.5 occurring

69   during non-bloom periods (Brzezinski et al., 2001). However, the number of D:P estimates,

70   due to a small number of Si uptake measurements and an even lower number of Si dissolution

71   measurements, is insufficient compared to the high variability observed regionally and

72   seasonally in the ocean which implies high uncertainty in the global D:P estimate and overall

73   on the marine silicon budget.

74   Diatoms are ecologically widespread and dominate the primary production in the Antarctic

75   Circumpolar Current (ACC), especially south of the Polar Front (PF), where their productivity

76   accounts for 1/3 of the global marine silica production (Pondaven et al. 2000; Buesseler et al.

77   2001). Consequently, this part of the Southern Ocean represents a key study area to improve

78   our understanding of the global biogeochemical cycles of both carbon and silicon. Biological

79   processes occurring in the Southern Ocean have indeed a significant impact on global

80   biogeochemistry. For example, the large H_4SiO_4 utilization by diatoms in the ACC, combined

81   to the global overturning circulation would determine the functioning of the biological pump

82   of low latitude areas by inducing a strong silicic acid limitation (Sarmiento et al., 2004). In the

83   Southern Ocean, a much larger depletion of silicic acid than nitrate in surface waters occurs

84   (Trull et al, 2001), which results from the action of a silicon pump, i.e. the preferential export

85   of BSi compared to particulate organic nitrogen (PON; Dugdale et al., 1995). This area is also

86   the largest High Nutrient Low Chlorophyll (HNLC) zone of the global ocean where dissolved

87   iron limitation plays a fundamental role in regulating the primary production and the carbon

88   cycle (De Baar et al., 2005; Boyd et al., 2007; Tagliabue et al., 2012). Indeed, phytoplankton

89   community structure and nutrient cycling could be largely controlled by Fe availability, with

90   highest growth rates located close to iron sources such as continental margins, island systems

91   and frontal regions (Blain et al., 2007; Tagliabue et al., 2012).

92   In this context, the KErguelen Ocean and Plateau compared Study (KEOPS) program,

93   consisting of two expeditions (late summer 2005 and early spring 2011), was conducted to

94   investigate a naturally iron-fertilized area located in the Indian sector of the Southern Ocean,

95   where the iron availability could potentially favor the carbon and silicon biological pumps

96   (Fig. 1; Blain et al., 2007). Two massive and complex blooms, which are clearly constrained

97   by the local bathymetry, are observed annually over the Kerguelen Plateau and contrast with

98   the HNLC character of surrounding waters (Pollard et al., 2002; Mongin et al., 2008). The

99   first KEOPS expedition (KEOPS-1, January-February 2005) has highlighted the impact of

100   natural iron fertilization on primary production and nutrient cycling, as well as the advantages

101   to study natural laboratories in the context of such ocean fertilization (Blain et al., 2008). The

102   general purpose of KEOPS-2 (October-November 2011) was to improve our knowledge about

103   the processes responsible for this iron fertilization and its impact on the seasonal variations of

104   the mechanisms controlling the primary production and carbon export. While the KEOPS-1

105   cruise was mainly directed towards the study of the bloom in the South-East area of the

106   Plateau, KEOPS-2 focused mainly on the bloom located North-East of the Kerguelen Islands

107   above the Kerguelen abyssal plain.

108   In this paper, we investigate the spatial and seasonal variability of silica production and

109   dissolution in the surface waters of the Kerguelen area. The specific objectives are the

110   following:

111   - Compare the Si cycle dynamics in contrasting productive environments such as the

112   southeastern Kerguelen Plateau bloom, the northeastern Kerguelen bloom in a stationary

113   meander southward the PF and the warmer waters located north of this front, relative to the

114   upstream HNLC area south-west of Kerguelen Islands, and identify controlling processes.

115   - Determine and quantify the seasonal evolution of processes which drive the Si

116   biogeochemical budget in the upper layer of the Kerguelen Plateau, using the ^{30}Si stable

117   isotope method (Nelson and Goering, 1977a; Fripiat et al, 2009) applied during KEOPS-2 and

118   other techniques of mass and isotopic balance used during KEOPS-1 (^{32}Si radiogenic tracer

119   incubations; Mosseri et al., 2008 and natural silicon isotopic composition, δ^{30}Si; Fripiat et al.,

120   2011a), in order to fully characterize the silicon cycle above the Kerguelen Plateau.

121   - Discuss the potential role of Fe on silica production – dissolution and on Si:N uptake ratios

122   in the context of the Silicic Acid Leakage Hypothesis (Brzezinski et al., 2002; Sarmiento et

123   al., 2004).

124 - Finally, compare our dataset with previous results in other productive regions of the global

125 ocean and discuss the different types of diatom dominated regimes.

126

127 **2 Material and methods**

128 **2.1 KEOPS-2 sampling campaign**

129 The KEOPS-2 cruise was conducted in the Indian sector of the Southern Ocean during the

130 austral spring 2011 (from October 10th to November 20th) on board the R/V Marion Dufresne

131 (TAAF/IPEV) and was focused on the iron-fertilized blooms observed around the Kerguelen

132 Plateau region. This plateau is a large area of relatively shallow seafloor that acts as a barrier

133 to the circumpolar flow of the ACC, forcing a large part of the current to pass north of the

134 plateau. The remaining flow passes south of the Kerguelen Islands and forms the jet of the PF,

135 which exhibits strong meandering and eddy activity (Park et al., 1998, 2008, Roquet et al.,

136 2009). As a consequence, the shallow region located south of Kerguelen Island represents a

137 zone of weak north-eastward circulation (Park et al., 2008; Roquet et al, 2009) and bears a

138 capacity of high chlorophyll *a* and BSi accumulation during phytoplankton blooms (Blain et

139 al., 2001; Mosseri et al., 2008; Mongin et al., 2008). Over the plateau, enhanced vertical

140 mixing associated to internal waves interact with the local bathymetry (Park et al., 2008) and

141 supply iron and macronutrients from depth to surface waters, enabling to fuel phytoplankton

142 bloom (Blain et al., 2007; Fripiat et al., 2011a).

143 The cruise included 8 long-term stations devoted to process studies with incubation

144 experiments (Fig. 1). Except for one station (E4E) where we were not able to measure silica

145 dissolution, Si fluxes were investigated in all these process-stations which characteristics are

146 presented in table 1:

147 - A HNLC reference station (R) located in deep waters south-west of Kerguelen Islands.

148 - The Kerguelen Plateau bloom reference station of KEOPS-1 (A3).

149 - A productive open ocean station (F) influenced by warmer Sub-Antarctic Surface Water,

150 located north of the Polar Front.

151 - A productive station (E4W) located in the plume of chlorophyll observed downstream of the

152 plateau and close to the jet induced by the PF.

153   - 4 stations (E1 to E5) constituting a pseudo-lagrangian survey located in a complex

154   recirculation zone in a stationary meander of the Polar front characterized by strong

155   mesoscale activity (Zhou et al., 2014).

156   **2.2   Sample collection, spike and incubation conditions**

157   The isotopic dilution technique adapted by Fripiat et al. (2009) from Corvaisier et al. (2005)

158   aims at simultaneously determining the rates of Si uptake (i.e. silica production) and of

159   biogenic silica dissolution in the same seawater sample. After spiking with a solution enriched

160   in ^{30}Si followed by incubation of the samples, the production rate is estimated from the

161   change in isotopic composition of the particulate phase (increase in ^{30}Si). Similarly, the

162   isotopic dilution (increase in ^{28}Si) in the ^{30}Si enriched seawater, due to the dissolution of

163   naturally ^{28}Si enriched BSi initially present, is used to estimate the dissolution rate.

164   Production and dissolution rates were determined at 7 and 5 depths respectively,

165   corresponding to different levels of Photosynthetically Active Radiation (PAR), from 75 % to

166   0.1 % of surface irradiance. Seawater was collected at defined depths in the euphotic layer

167   using Niskin bottles mounted on a CTD-rosette. For each depth, 5 l of seawater were sampled.

168   1 l was subsampled to obtain a natural silicon isotopic standard (i.e. not spiked with ^{30}Si) to be

169   processed along with the samples to correct for the matrix effect and mass bias during isotopic

170   analysis (Fripiat et al., 2009). These unspiked samples were immediately filtered on 0.8 μm

171   Nuclepore polycarbonate membranes to separate biogenic silica from silicic acid. The

172   membrane was dried at 50 °C overnight and the filtrate was directly preconcentrated (see

173   section – *Sample preparation and isotopic measurements*) and stored at room temperature in

174   the dark.

175   The remaining seawater volume was subsampled in 2 l aliquots spiked with H$_4$^{30}SiO$_4$-

176   enriched solution (99 % ^{30}Si). Aliquots devoted to production measurements were spiked with

177   a spike contribution representing usually less than 10 % of natural concentrations to minimize

178   the perturbation of the natural DSi contents (Nelson & Goering, 1977a). In order to improve

179   the detection limit of the method for dissolution, a second 2 l aliquot was spiked by adding

180   ^{30}Si in the same amount as natural DSi (i.e. DSi spike addition at 100 % of the initial DSi).

181   This provided sufficient sensitivity for the isotopic measurements of dissolution (see section –

182   *Accuracy of the model, detection limit and standard deviation*).

183   Immediately after spike addition and gentle mixing, 1 l was filtered following the same

184   procedure than for the unspiked standard, to determine the initial conditions (t_0). The second

185   half of the sample was poured into polycarbonate incubation-bottles and incubated under light

186   conditions simulating those prevailing *in situ* for 24 h (10 % spiked samples) and for 48 h

187   (100 % spiked samples). Deck-incubators were fitted with blue plastic optical filters to

188   simulate the light attenuation of the corresponding sampling depths, and temperature was

189   regulated by circulating surface seawater. At the end of the incubation period, samples were

190   filtered and treated as described above to characterize the final conditions of the incubation

191   (t_{24} or t_{48}).

192   **2.3   Sample preparation and isotopic measurements**

193   Preconcentration of H_4SiO_4 in the seawater samples (for both production and dissolution

194   measurements) was applied on-board to increase the Si:salinity ratio, because the maximum

195   salinity of the solution that can be introduced in the mass spectrometer is about 2 ‰ (Fripiat

196   et al., 2009). This step was achieved using a protocol adapted from the MAGIC method (Karl

197   & Tien, 1992; Reynolds et al., 2006). The H_4SiO_4 in seawater was scavenged by the brucite

198   precipitate ($Mg(OH)_2$) obtained by adding 1 ml of 14 N NaOH to the 1 l of seawater sample

199   and strong stirring. The precipitate was recovered by decantation and centrifugation, and was

200   then dissolved in 3 ml of 3 N HCl.

201   In the shore based laboratory, polycarbonate membranes (t_0, t_{24} and t_{48} for both production and

202   dissolution measurements) were digested in one step using a protocol adapted from

203   Ragueneau et al. (2005) with 4 ml of 0.2 N NaOH during 40 min at 100 °C to hydrolyse BSi.

204   Samples were then neutralized with 1 ml of 1 N HCl to stop the reaction.

205   An aliquot of the solutions obtained after preconcentration and digestion was used to

206   determine colorimetrically the DSi and BSi concentrations, following the method of

207   Strickland and Parsons (1972). The remaining sample was diluted to 100 ppb Si in a 2 %

208   HNO_3 solution to determine the initial and final Si isotopic composition of the dissolved and

209   particulate phases using a Element 2 (Thermo-Fischer) HR-SF-ICP-MS (High Resolution –

210   Sector Field – Inductively Coupled Plasma – Mass Spectrometer) with the same configuration

211   used by Fripiat et al. (2009). The sequence of analysis consists in: blank – natural standard –

212   spiked sample 1 – natural standard – spiked sample 2 – natural standard – spiked sample 3 –

213   natural standard – blank. The average of the two blanks were subtracted to each standard and

214   sample. To test whether our dissolution measurements were biased by a ^{30}Si contamination
215   linked to a possible memory effect in the HR-SF-ICP-MS, we compared the average
216   composition of the first natural standards (i.e., without contamination from memory effect, n
217   = 55) with the composition of natural standards analyzed after a spiked sample (n = 102).
218   There was no significant difference between natural standards passed before and after a 100
219   % DSi spiked sample (T-test, p-value <0.001). We can thus exclude significant memory effect
220   when applying the analytical sequence described above.

221

222   3   Results

223   3.1   Accuracy of the model, detection limit and standard deviation

224   To estimate the production and dissolution of biogenic silica (ρSi and ρDiss, respectively),
225   two different models are available: the linear one-compartmental model described by Nelson
226   and Goering (1977a, b) and the non-linear two-compartmental model described in de
227   Brauwere et al. (2005) and Elskens et al. (2007). In the latter, both isotopic composition and
228   concentration changes occurring during the incubation time are taken into account to estimate
229   production and dissolution rates simultaneously. Lack of consideration of these changes could
230   induce significant biases in the estimated fluxes (Elskens et al., 2007). In this model the fluxes
231   are calculated by resolving a system of 4 equations given by:

232    $$[DSi]_t = [DSi]_{t0} + (\rho Diss - \rho Si) \times t \tag{3}$$

233    $$[BSi]_t = [BSi]_{t0} \times (\rho Si - \rho Diss) \times t \tag{4}$$

234    $$æDSi_t = æDSi_{t0} \times \left(1 + \frac{\rho Diss - \rho Si}{[DSi]_{t0}} \times t\right)^{\frac{\rho Diss}{\rho Si - \rho Diss}} \tag{5}$$

235    $$æBSi_t = \frac{æDSi_{t0} \times [DSi]_{t0}}{[BSi]_{t0} + (\rho Si - \rho Diss) \times t} \times \left(1 - \left(1 + \frac{\rho Diss - \rho Si}{[DSi]_{t0}} \times t\right)^{\frac{\rho Si}{\rho Si - \rho Diss}}\right) \tag{6}$$

236   where [BSi] and [DSi] are the dissolved silicon and biogenic silica concentrations (in µmol l^{-}
237   ^{1}); æBSi and æDSi are the abundance in excess of ^{30}Si (measured minus natural abundances)
238   in the particulate and dissolved phase respectively; the subscribes t0 and t refer to the initial
239   and final incubation values.

240   The best solution is found numerically by optimizing parameter values (ρSi and ρDiss) and

241   minimizing the cost function (weighted sum of squared differences between calculated and

242   measured variables, [BSi], [H_4SiO_4], æBSi and æDSi for the four equations simultaneously;

243   de Brauwere et al., 2005; Elskens et al., 2007).

244   The relevance of the 2 models against a given data set has already been discussed by Elskens

245   et al. (2007) and Fripiat et al. (2011b). Taking into account these considerations, and after

246   testing the accuracy and the sensitivity of each model, we use preferentially the non-linear 2

247   compartmental model to estimate the biogenic silica production and dissolution during

248   KEOPS-2. This model was tested according to the four criteria and the residual of the cost

249   function was checked to follow a Chi² distribution as detailed in Elskens et al. (2007). Due to

250   unexpected sampling problems on-board, we were not able to measure $[DSi]_t$. Thus, in

251   addition to the biogenic silica production and dissolution rates, this variable was also

252   estimated by the model (Eqs. 3-6). Under these conditions, one degree of freedom is lost but

253   the system remains identifiable with 3 unknowns and 4 equations.

254   KEOPS-2 took place during the onset of the blooms, the biogenic silica production rates were

255   quite high and far above the detection limit, except for 3 depths of the HNLC reference station

256   (R) and for the deepest value at each station (0.01 % PAR attenuation depth, 8 samples).

257   However, since biogenic silica dissolution rates were expected to be low in early spring, it is

258   essential to determine the limit of detection for the ^{30}Si isotopic dilution.

259   In most cases, final æDSi were significantly different from initial æDSi (paired T-test, p-value

260   < 0.001). The detection limit for isotopic dilution was then estimated as being the lowest

261   difference between initial and final ^{30}Si isotopic abundances (ΔæDSi) measurable by the

262   instrument. Every æDSi solutions have been analyzed in duplicates with a pooled standard

263   deviation of 0.32 % (n = 35). In addition, we analyzed the same in-house standard several

264   times during every analytical session. This solution was a 10 % spiked seawater from

265   Southern Ocean analyzed since several years with a æDSi at 11.83 ± 0.43 % (n = 40). The

266   relative standard deviation (RSD) on æDSi of this standard solution is 0.43 % (n = 40) and

267   represents the long-term reproducibility of HR-SF-ICP-MS measurements. Therefore, each

268   KEOPS-2 incubation with a ΔæDSi between t_0 and t_{48} higher than this RSD was considered to

269   be significantly different from zero, and hence above the detection limit. This was the case for

270   almost all the KEOPS-2 dataset (see e.g. Fig. 2), except for 7 values showing a change in ^{30}Si

271 abundance below the detection limit. This included 4 samples from the HNLC reference
272 station R where biological activity was extremely low.

273 Due to time and sampled water volume constraints, the sampling strategy adopted for
274 KEOPS-2 gave the priority to highest vertical resolution instead of replicate incubations.
275 Since only the analytical reproducibility was taken into account in the model, the standard
276 deviations on Si uptake and dissolution rates were likely to be underestimated. Therefore we
277 will use a theoretical relative precision for the whole incubation experiments of 10 %, as
278 estimated for Si uptake rates by Fripiat et al. (2009).

279 ## 3.2 Physical, chemical and biological parameters

280 The vertical structure of upper layer waters in the area was characteristic of the Antarctic
281 Surface Water in the vicinity of the Polar Front (Park et al., 1998, 2008). The Winter Water
282 (WW), identified by the minimum of temperature centered around 200 m, was capped by a
283 homogeneous mixed layer (ML) induced by seasonal stratification. The boundary between the
284 surface ML and the WW is usually marked by a strong seasonal pycnocline. However, at
285 some stations, the stratification of the surface layer was relatively complex and showed two
286 successive discontinuities evidenced by two different density gradients as indicated in Fig. 3.

287 During KEOPS-2, the surface ML depth, defined by the density difference of 0.02 from the
288 surface (Park et al, in prep.), showed a large variability between stations (Fig. 3). A strong and
289 shallow stratification was measured north of the polar front, while wind events induced weak
290 stratification and deep ML in the stations above the plateau and in the HNLC area. Stations in
291 the recirculation zone (E1 to E5) supported a complex stratification due to their highly spatial
292 and temporal dynamic and were characterized by 2 distinct density discontinuities.

293 All the stations located south of the Polar Front had quite homogeneous Chl-a, BSi and DSi
294 stocks from the surface to the deepest density discontinuity (below the so-called ML; Fig. 3).
295 North of the Polar Front, these stocks were higher at the surface and decreased with depth
296 (Fig. 3c). Stations A3 and E4W present similar BSi and DSi surface concentrations (Fig. 3e,
297 g). At these 2 stations, DSi concentrations increase gradually while Chl-a and BSi decrease
298 drastically below the deepest density discontinuity. Station R contrasted from the latter
299 stations by its low BSi, low Chl-a content and relatively high DSi concentrations, confirming
300 its HNLC character (Fig. 3a). During the lagrangian survey (stations E1, E3, E4E and E5), we
301 observed a DSi depletion from ≈15 to ≈10 µmol l^{-1} in surface waters, an increase of Chl-a

302   concentrations from < 1 to > 1 mg m^{-3} and a doubling of the BSi content from ≈1.5 to > 3

303   μmol l^{-1} (Fig. 3b, d, f, h). Such temporal variations were mainly driven by diatom production

304   as described below.

305   **3.3   Biogenic silica production and dissolution rates**

306   Silica production rates were quite homogeneously distributed in the euphotic layer with an

307   exception for the station F located north of the Polar Front where it decreases progressively

308   with depth (Fig. 4a). Surface ρSi varied from 0.036 ± 0.003 μmol l^{-1} d^{-1} (R in the HNLC area)

309   to 1.28 ± 0.12 μmol l^{-1} d^{-1} (A3, above the Plateau). All over the study area, Si uptake rates

310   reached very low values at the base of the euphotic layer. Note that the same decreasing trend

311   was also observed in primary production experiments performed in parallel (see e.g. Cavagna

312   et al., in prep.).

313   BSi dissolution rates were considerably lower than Si uptake rates except in the HNLC area

314   (R) and at station E3 where ρSi was in the lower range of the KEOPS-2 dataset. Vertical

315   profiles of ρDiss (Fig. 4b) were quite homogeneous from the surface to the base of the

316   euphotic layer and did not increase at depth. This indicates that, the physical and

317   biogeochemical processes affecting BSi dissolution did not vary significantly over the water

318   column. This is also consistent with the low accumulation of biogenic silica observed at depth

319   in spring (Lasbleiz et al., 2014) which contrasts with the occurrence of deep BSi maxima at

320   the end of summer (Mosseri et al., 2008). Moreover, silica dissolution rates were not

321   significantly different between bloom stations, and were comparable to those measured by

322   Brzezinski et al. (2001) for the same season in the Pacific sector and by Beucher et al. (2004)

323   and Fripiat et al. (2011b) for the end of summer in the Australian sector.

324   As silica production was close to zero below the euphotic layer, all the vertically integrated

325   values presented in table 2 were calculated from 100 % to 1 % of the surface PAR. The

326   integrated Si uptake rates (∫ρSi) varied from 3.09 ± 0.01 mmol m^{-2} d^{-1} (R, in the HNLC area)

327   to 47.9 ± 0.4 mmol m^{-2} d^{-1} (A3, above the Plateau), and were among the highest reported so

328   far in the Southern Ocean (see review in Fripiat, 2010). Integrated BSi dissolution rates

329   (∫ρDiss) were generally much lower than integrated production rates with values ranging from

330   3.79 ± 0.03 mmol m^{-2} d^{-1} north of the Polar Front (F) to 9.99 ± 0.03 mmol m^{-2} d^{-1} at E3.

331   Because ρDiss did not vary over depth, or between stations, integrated dissolution estimates

332 were correlated with the depth of the euphotic layer (Ze), with higher values in stations with

333 deeper Ze, e.g. E1 and E3 (R^2 = 0.83, not shown).

334 Net production rate of BSi in the euphotic layer ($\int \rho Si_{net}$) represents the difference between

335 gross silica production and dissolution rates (Fig. 5) and could be associated to an uptake of

336 "new-H_4SiO_4" i.e. uptake that does not come from remineralisation processes within the ML.

337 As for the net primary production, the net silica production could be defined as the part of the

338 BSi that accumulates in the surface layer during the productive period, which would then be

339 potentially available later for export to the mesopelagic layer (Brzezinski et al., 2001;

340 Quéguiner, 2013). During the pseudo-lagrangian survey, net silica production was quite low

341 during the first 2 visits (E1 and E3 with respectively 9.6 ± 0.1 and 0.5 ± 0.1 mmol m^{-2} d^{-1}) and

342 reached the maximal value at the last visit (E5, 20.5 ± 0.2 mmol m^{-2} d^{-1}). The highest net

343 production rate was observed above the Kerguelen Plateau (A3, 43.4 ± 0.4 mmol m^{-2} d^{-1}). In

344 the HNLC area (Station R), silica dissolution was higher than silica production, leading to a

345 negative $\int \rho Si_{net}$(-1.78 ± 0.02 mmol m^{-2} d^{-1}).

346 **3.4 Specific rates of production and dissolution**

347 The specific Si uptake rate (VSi, d^{-1}) and dissolution rate (VDiss, d^{-1}) give the fraction of the

348 BSi pool produced or dissolved in one day as follows:

349 $$VSi = \frac{\rho Si}{[BSi]} \qquad (7)$$

350 and $$VDiss = \frac{\rho Diss}{[BSi]} \qquad (8)$$

351 VSi is mainly impacted by nutrient and/or light limitation (Frank et al., 2000; Claquin et al.,

352 2002) and by the diatom community composition (Leynaert et al., 2004). During KEOPS-2,

353 VSi values (profiles not shown) presented the same decreasing trends with depth as Si uptake,

354 which is consistent with an impact of light limitation on silica production. Globally, relatively

355 high "integrated specific Si-uptake rates" ($\int$VSi, calculated by the averaged integrated ρ

356 divided by the integrated BSi) prevailed for KEOPS-2 ($\approx$0.1 to $\approx$0.3 d^{-1}; table 2). Such values

357 are not different from those of nutrient-replete diatoms growing in the open ocean zone of the

358 Southern Ocean (Brzezinski et al., 2001). By contrast, the HNLC area showed a $\int$VSi value

359 below 0.1 d^{-1}, suggesting non-optimal conditions for the growth of diatoms and/or artifact of

360   siliceous detritus, which is important in other HNLC regions (e.g. Krause et al., 2010; Fripiat

361   et al., 2011b).

362   ∫VDiss varied around one order of magnitude during KEOPS-2 with low specific rates in

363   productive stations (e.g. 0.03 d^{-1} above the Plateau), and higher values in the HNLC area (up

364   to 0.15 d^{-1}). Interestingly, E3 showed unexpected high ∫VDiss (0.12 d^{-1}; table 2).

365

4   Discussion

4.1   Seasonality of the balance between silica production and dissolution

368   The D:P ratios integrated between the surface and the 1 % PAR attenuation depth (∫D:∫P; also

369   summarized in table 3) are presented in figure 5. At the HNLC reference station R, the ∫D:∫P

370   value >1 indicates that the integrated dissolution rate exceeds the measured integrated

371   production rate (note that both fluxes were very low at R). This situation leads to a net loss of

372   biogenic silica by dissolution in the euphotic zone and suggests that a short development of

373   diatoms could have occurred before our sampling. This observation is in accordance with the

374   high barium excess measured between 200 and 400 m at R (Jacquet et al, 2014), indicating a

375   high carbon mineralization activity in the mesopelagic zone which could be likely associated

376   to a surface production event prior sampling. High ∫D:∫P values have already been measured

377   occasionally in the Southern Ocean during the summer bloom (review in Tréguer and De La

378   Rocha, 2013).

379   In the Kerguelen bloom area, ∫D:∫P ratios ranged from 0.09 (station A3) to 0.95 (station E3)

380   and depended on the stage of the blooms. The ∫D:∫P ratios were relatively high at stations

381   visited in the beginning of the cruise, indicating that a significant fraction of silica was

382   recycled in the surface waters in early spring, and then decreased as the bloom took place.

383   The highest ∫D:∫P ratio occurred at station E3. This station was characterized by a low BSi

384   stock (83.6 mmol Si m^{-2}), a low integrated BSi production rate (10.5 mmol Si m^{-2} d^{-1}

385   integrated over the euphotic layer; table 2), a dissolution rate close to the mean for all stations,

386   and high specific dissolution rate. This may evidence a higher relative proportion of detrital

387   silica free of organic matter at this station which could be due to stronger bacterial and/or

388   grazing activities inducing a top-down control on diatom growth. Without considering E3,

389   ∫D:∫P ratios decreased progressively from E1 to E5 and showed low values at the most

390   productive stations E4W, A3 and F. Here, ∫D:∫P ratios were similar to those measured in

391   nutrient-replete conditions such as productive upwelling regions (Brzezinski et al., 2003).

392   High ∫D:∫P ratios in winter and in early spring indicate that silica dissolution is sufficient to

393   sustain a large fraction of the low Si uptake rates observed during non-bloom conditions and

394   during the bloom onset, i.e. when primary production is still low. Indeed there is a temporal

395   decoupling between silica production and dissolution since the dissolution kinetic is slow. It is

396   only after diatom death and removal of their protecting organic coating by micro-organisms

397   that the silica frustules can dissolve (Kamatani, 1982; Bidle and Azam, 1999; Bidle et al.,

398   2003). By contrast, the progressive decrease of the ∫D:∫P values implies that the majority of

399   gross silica production is sustained by the silicic acid pool supplied from below (winter water)

400   as the bloom develops. This pool can be regarded as the "new" Si reservoir, similar to nitrate

401   for N. Thus, we observe a seasonal shift from Si uptake behaving mainly as a regenerated

402   production before the bloom onset, when silica production is still very low, and then behaving

403   more like a new production during bloom, when we observe higher Si uptake rates.

404   An opposite shift at the end of the productive period was suggested by Brzezinski et al. (2001)

405   in the upwelling system of the Monterey Bay with ∫D:∫P ratios increasing following the bloom

406   development. In this case, higher ∫D:∫P values were associated to an increase of the relative

407   proportion of detrital BSi in the water column. Similarly, the occurrence of an accumulation

408   of dissolving BSi in subsurface following productive periods inducing a net loss of BSi in late

409   summer (∫D:∫P = 1.7) was already identified in the Australian sector of the Southern Ocean

410   (Fripiat et al., 2011b). Since KEOPS-2 took place at the start of the bloom and since there was

411   no silica dissolution rate measured from KEOPS-1, such increase of ∫D:∫P ratio in the

412   Kerguelen area at the end of the blooming season has not been observed but will be discussed

413   in section 4.5.

414   Because silica dissolution profiles were not significantly different from each other between all

415   the KEOPS-2 bloom stations (Fig. 4b), it can be ruled out as a process explaining the

416   variability in ∫D:∫P ratios. The observed decreasing trend of ∫D:∫P ratios was actually mainly

417   driven by the increase of BSi production rates (from 3.09 ± 0.01 to 47.9 ± 0.4 mmol Si m^{-2} d^{-}

418   ^{1}) and by the accumulation of living diatoms with high specific Si uptake rates in the euphotic

419   layer (table 2).

420   The fraction of silica production supported by new silicic acid is estimated by $1-\int D:\int P$. During

421   KEOPS-2 it ranged from -0.58 in the HNLC station, where we observed a net loss of biogenic

422   silica, to a maximum of 0.91 above the plateau, where maximum production rates were

423   recorded (A3, table 3). When plotting $1-\int D:\int P$ vs. gross silica production rate, Brzezinski et al.

424   (2003) found that 8 regional estimates of this parameter representing a large range of ocean

425   environments, fall along an hyperbolic curve and thus it might be possible to predict the

426   strength of the silicon pump in a system based on its mean silica production. To obtain a zero-

427   intercept of the curve satisfying the assumption that when the fraction of silica production

428   supported by new silicic acid approaches 0, the production must also be 0, we have plotted the

429     $1-\int D:\int P$ as a function of the net silica production (instead of the gross production in Brzezinski

430   et al., 2003). Since these two variables are not fully independent, the equation of the model

431   matching all the data follows a rectangular hyperbola (Fig. 6). This fitting has been obtained

432   on KEOPS-2, Brzezinski et al. (2003) and Fripiat et al. (2011b) data.

433   Using figure 6, we can identify several parameters characterizing the distribution of both

434   KEOPS-2 stations and other oceanic regions. The $1-\int D:\int P_{max}$ is centered around 1 as it is not

435   possible to have more than 100 % of silica production supported by new-H_4SiO_4. The $K_{\rho Net}$

436   (5.89 ± 2.24 mmol m^{-2} d^{-1}) represents the value of net silica production at which the system

437   shifts from a regenerated to a new biogenic silica production (i.e., $1-\int D:\int P = 0.5$). In KEOPS-2

438   stations showing a net silica production below $K_{\rho Net}$, the development of diatoms is mainly

439   controlled by recycled sources of silicon, while above this value, the supply of new H_4SiO_4 is

440   the main source of nutrients for biogenic silica production. It is important to keep in mind that

441   this model is mainly governed by the dependency of its two variables and thus, we cannot use

442   it to make predictions about the silicon cycle functioning of stations where only one of the

443   two parameters was estimated (e.g. net silica production estimated from the change in BSi

444   concentrations). It however allows us to sort KEOPS-2 stations into specific groups and to

445   compare them with other oceanic regions. For example, figure 6 is remarkably helpful to

446   differentiate stations with low net production rates (x-axis) that have very variable fraction of

447   new Si production (y-axis).

448   KEOPS-2 stations follow the same trend as that of Brzezinski et al. (2003) and encompass

449   almost the full range of variability observed in very contrasting oceanic regions (e.g. HNLC,

450   oligotrophic, coastal upwelling, river plume). They can be sorted in 3 functional groups:

451　- The "low activity stations" group includes the HNLC reference station R and station E3 that

452　showed a net loss of BSi with negative values of $\int \rho Si_{net}$ or close to 0 (Fig. 5; table 2). In Fig.

453　6, the HNLC station falls in the negative part of the hyperbolic curve, close to stations mainly

454　characterized by detrital BSi dominance and where a release of silicon from dissolving BSi

455　takes place following a productive period (e.g. the late summer SAZ-Sense station P2 located

456　in the Polar Front Zone; Fripiat et al., 2011b). Despite its low iron concentration, the high

457　$\int D:\int P$ ratio observed at R suggests that a short development of diatoms could have occurred

458　before our sampling in agreement with Jacquet et al. (2014) and Dehairs et al. (in prep.). This

459　kind of low diatom production in the HNLC area surrounding the Kerguelen Plateau has

460　already been suggested at the end of summer by Mosseri et al (2008). Since net silica

461　dissolution is not sustainable, the values measured at R should necessarily represent

462　conditions that prevail on a short period of time. Production and dissolution rates are indeed

463　snapshot measurements over 24 h or 48 h. Although H_4SiO_4 concentrations were not limiting

464　in surface waters, E3 was characterized by very low silica production that could be

465　exclusively sustained by recycled silicic acid (1-$\int D:\int P = 0.05$) and seemed to have approached

466　steady state conditions as siliceous biomass cannot increase in a system supported solely by

467　regenerated silicic acid (Brzezinski and Nelson, 1989). This situation could be the result of a

468　previous attempt to bloom that would have aborted due to the destabilization of the ML.

469　- The "starting-bloom" group is represented by station E1 that has been visited in the

470　beginning of the KEOPS-2 cruise (early November). Although carbon incubation experiments

471　reveal that the bloom began to grow at this station (Cavagna et al., in prep.), low Si uptake

472　(Fig. 4a) and low net-silica production (Fig. 5) were still observed. A moderate 1-$\int D:\int P$ ratio

473　(0.58) indicates that BSi production at E1 is controlled both by new and regenerated sources

474　of H_4SiO_4.

475　- The "spring-bloom" group includes stations holding a strong capacity for BSi accumulation,

476　i.e. with low dissolution rates and high net silica production rates. Figure 4a allows us to

477　distinguish between stations from the lagrangian study E4E and E5, with only moderate

478　surface ρSi values (respectively 0.62 ± 0.06 µmol l^{-1} d^{-1} and 0.57 ± 0.06 µmol l^{-1} d^{-1}) and

479　$\int D:\int P$ ratio close to 0.3 (table 3); and stations A3, F and E4W showing particularly high

480　surface production rates (> 1 µmol l^{-1} d^{-1}) and $\int D:\int P$ ratio close to 0.1 (table 3). Blooms with

481　such a low $\int D:\int P$ ratio have the potential to accumulate a large fraction of BSi production

482　and/or export a large amount of BSi into the deep ocean (Quéguiner, 2013; Tréguer and De La

483　Rocha, 2013). Despite their location on both sides of the Polar Front and in different part of

484   the Kerguelen bloom, stations E4W and F fall close to each other along the hyperbolic curve

485   (Fig. 6). Consequently, they should operate in a comparable way in term of silica production

486   dynamic which is quite similar to the average value of PFZ spring bloom conditions measured

487   by Brzezinski et al. (2001). So, even though complex physical settings (Park et al., in prep.)

488   are very different between E4W (which is not part of PF with high surface DSi concentration

489   of 17 µmol l^{-1}) and F (with lower surface DSi concentration of 6 µmol l^{-1}) diatom production

490   regime behave as typical PFZ stations. This was also observed with carbon export and

491   mesopelagic remineralization by Jacquet et al. (2014). Compared to F and E4W, A3 is highly

492   active in term of silica production and can be compared to the Amazon river plume and

493   coastal upwelling systems such as Monterey Bay or Peru. This highlights once again the

494   exceptional character of diatoms-dominated ecosystems sustained by natural iron fertilization

495   in the Southern Ocean.

496   **4.2   Decoupling between Si, C and N cycles in the Kerguelen area**

497   In the Kerguelen area, the high NO_3^- concentrations in surface waters compared to H_4SiO_4

498   depletion observed annually at the end of the bloom period suggest a strong decoupling

499   between the seasonal consumption of these two nutrients (Mosseri et al., 2008). This situation

500   could be partly induced by differential recycling processes between Si and N strengthening

501   the silicon pump. Si is thus primarily exported to deeper water through sinking of biogenic

502   silica while PON is mostly recycled in the ML and used as nitrogen source for the

503   development of new phytoplankton organisms including diatoms. Since organic matter is

504   more quickly and efficiently remineralized compared to silica, this decoupling also occurs

505   between Si and C.

506   The strength of the silicon pump could be investigated by comparing the Si:C and Si:N

507   uptake-ratios. In this study, we use only the gross uptake ratios ($\int\rho Si{:}\int\rho N$ and $\int\rho Si{:}\int\rho C$),

508   calculated respectively as:

509   $$\int\rho Si{:}\int\rho N = \frac{\rho Si}{\rho(NO_3^- + NH_4^+)} \tag{9}$$

510   and $$\int\rho Si{:}\int\rho C = \frac{\rho Si}{gross\ \rho C} \tag{10}$$

511   which reflect only the stoichiometry of phytoplankton nutrient uptake. We will not consider

512   net uptake ratios that could be calculated but would be biased by the significant rates of

513   nitrification estimated at all KEOPS-2 stations (see Cavagna et al., in prep. and Dehairs et al.,

514   in prep.). Note that both $\int\rho Si:\int\rho C$ and $\int\rho Si:\int\rho N$ uptake ratios are underestimates of actual

515   diatom uptake ratios because of the simultaneous C and N uptake by non-siliceous organisms.

516   Diatoms growing in nutrient replete conditions present Si:C and Si:N elemental ratios around

517   0.13 (from 0.09 to 0.15) and 1 (from 0.8 to 1.2) respectively, with the variability of these

518   ratios depending on diatom species, size classes and growth rates (Brzezinski, 1985; Martin-

519   Jézéquel et al., 2000).

520   Si:C and Si:N uptake ratios are strongly impacted by co-limitations which alter growth rates

521   and in most cases increase silicification processes, and thus lead to higher uptake ratios

522   (Claquin et al., 2002; Leynaert et al., 2004; Bucciarelli et al., 2010). During the KEOPS-2

523   study, $\int\rho Si:\int\rho C$ and $\int\rho Si:\int\rho N$ uptake ratios vary from 0.10 to 0.38 and from 0.32 to 1.51

524   respectively (table 3).

525   In our study, these variations could not be explained by limitation from macronutrient (such

526   as silicic acid) as already proposed by Nelson and Tréguer, (1992) and Quéguiner, (2001).

527   Indeed, KEOPS-2 took place at the beginning of the growth period (October-November) and

528   a bloom onset was observed above the Plateau (Blain et al., in prep.). It is thus not surprising

529   that macronutrient concentrations in the surface layer were not limiting for diatom growth (cf.

530   Cavagna et al., in prep. for N uptake). For silicic acid, kinetic experiments conducted during

531   the cruise at all sites demonstrated the lack of response of phytoplankton to H_4SiO_4

532   enrichment (data not shown). Indeed, at all stations, mixed layer silicic acid concentrations

533   were high (from 6.2 to 18.5 $\mu mol.l^{-1}$; Fig. 3) preventing limitation of biogenic silica

534   production by H_4SiO_4 availability as V_{Si} at ambient DSi were always similar to V_{max}, the

535   maximum uptake rate achievable when Si is not limiting (data not shown).

536   Results from a previous cruise in the same area (austral spring 1995) already highlighted the

537   crucial role played by the light-mixing regime on the control of diatom growth in the nutrient

538   replete waters (Blain et al., 2001). Light-limitation also takes part in the decoupling between

539   Si, N and C cycles by decreasing the growth rate and consequently increasing Si:N and Si:C

540   uptake-ratios (Claquin et al., 2002). At all stations the $\rho Si:\rho C$ uptake ratios increase slightly

541   with depth and reach a maximum at the bottom of the euphotic layer (data not shown), in

542   agreement with the fact that C assimilation is light-dependent through photosynthesis while

543   silicification processes mainly involves energy coming from respiration (Martin-Jézéquel et

544   al., 2000; Claquin et al., 2002). However, because Si uptakes reach very low values at the

545 base of the euphotic layer (Fig. 4a), our data suggest that BSi production rates were not fully

546 independent of light levels and that there was a close coupling between C and Si assimilation

547 processes (see Cavagna et al., in prep. for carbon uptake). This coupling of ρSi with light was

548 also observed in other regions as the Equatorial Pacific and the North Pacific Subtropical gyre

549 by Krause et al. (2011). Note however that this is not in contradiction with Claquin et al.

550 (2002) given the different time scales of the two studies.

551 Limitation by trace metals (especially iron) also alters the stoichiometry of phytoplankton

552 nutrient uptake and its elemental composition and, eventually, contributes to the decoupling

553 between Si, N and C cycles. From bottle enrichment experiments, it has been argued that

554 diatoms have higher Si:N uptake ratios under Fe stress (Takeda 1998; Hutchins and Bruland

555 1998; Franck et al., 2000). Interestingly, relatively high $\int\rho Si:\int\rho N$ ratios were measured for the

556 Kerguelen spring bloom (table 3), with the highest value above the Plateau (1.5, station A3)

557 although this area was naturally Fe-enriched (Sarthou et al., in prep.; Queroue et al., in prep.).

558 In the KEOPS-2 productive stations, diatoms can take up more H_4SiO_4 compared to nitrogen

559 and carbon. Indeed, these organisms are known to store silicic acid in their vacuoles or linked

560 to other intracellular components (Martin-Jézéquel et al., 2000, Hildebrand, 2008), or could

561 be more silicified. By contrast, 3 stations showed low $\int\rho Si:\int\rho N$ uptake ratios (0.44, 0.74 and

562 0.32 for R, E3 and F respectively). Lower Si:N and Si:C integrated uptake ratios in these areas

563 might be partly due to changes in phytoplankton composition. By measuring phytoplankton

564 pigment composition in the HNLC station, Lasbleiz et al. (2014) estimated a lower

565 contribution of microphytoplankton due to a higher proportion of nanophytoplankton

566 organisms such as nanoflagellates. Thus, since the phytoplankton community at R may

567 contain a significant fraction of non-siliceous organisms, the C and N uptake ratios were not

568 solely prescribed by diatoms and thus could explain the low $\int\rho Si:\int\rho N$ uptake ratios observed.

569 However, the higher concentrations in fucoxanthin over the other pigments at all other

570 stations clearly evidence the dominance of large diatoms in the Kerguelen blooms (Lasbleiz et

571 al., 2014). The very low $\int\rho Si:\int\rho N$ uptake ratios estimated at F could not result from a

572 dominance of non-siliceous phytoplanktonic organisms but likely from different diatom

573 communities showing contrasted degree of silicification and adapted to the specific

574 hydrological and biogeochemical conditions occurring north of the Polar Front. Indeed,

575 previous studies in the Southern Ocean have already shown that diatom community

576 composition could explain more differences in silicification than physiological responses to

577 environmental factors such as iron concentration (Baines et al., 2010; Assmy et al., 2013).

578   Thus, at a seasonal scale and above the plateau, the combination of this increased Si uptake

579   and nitrogen regeneration processes including nitrification (see e.g. in Cavagna et al., in prep.;

580   Dehairs et al., in prep.) in the beginning of the bloom, and preferential recycling of organic

581   matter at the bloom offset helps to explain the depletion of most of the Si from surface layer

582   observed between early spring (18.7 µmol l^{-1}, averaged in the upper 80 m at station A3,

583   KEOPS-2) and the end of summer (1.9 µmol l^{-1}, averaged in the upper 80 m at station A3,

584   KEOPS-1; Mosseri et al., 2008), while nitrate remains abundant (23 µmol l^{-1}, averaged in the

585   upper 80 m at station A3, KEOPS-1; Mosseri et al., 2008). Fe-replete diatom assemblages,

586   such as those found at A3 (Sarthou et al., in prep.), will deplete silicic acid from the water

587   column before nitrate. Such silicon pump above Kerguelen Plateau would then not be driven

588   solely by Fe-limitation contrary to incubation experiments from coastal upwelling systems

589   (Hutchins and Bruland, 1998). Indeed, Fe enrichments in bottle experiments fertilise on short

590   time scale (days) a diatom community that is not adapted to higher Fe levels. Here, by

591   comparing ∫ρSi:∫ρN uptake ratios on different natural communities adapted to their specific

592   ambient Fe levels, our results suggest that natural Fe fertilisation might favour diatoms with

593   higher Si:N ratios. Above the Kerguelen Plateau, diatoms seem to maintain a relatively higher

594   degree of silicification until the demise of the bloom, since Mosseri et al. (2008) observed the

595   same range of ∫ρSi:∫ρN at A3 (1.6 ± 0.5, n=3).

596   If confirmed in other naturally fertilized regions, these observations may have great

597   implications in our understanding of the past and future functioning of the Southern Ocean

598   and its role in the regulation of climate. Indeed, the silicon pump occurring in the ACC results

599   in an Antarctic Surface Water (AASW) relatively replete in NO_3^- but strongly depleted in

600   H_4SiO_4 as observed by Blain et al. (2007) and Mosseri et al. (2008) in the Kerguelen region.

601   This property is then exported toward lower latitudes by the Antarctic Intermediate Water

602   (AAIW) and Subantarctic Mode Water (SAMW) (Sarmiento et al., 2004), currently favouring

603   non siliceous organisms production in these regions. Thus, any change in Si:N uptake ratios

604   south of the region of AAIW and SAMW formation might in turn modify diatom productivity

605   at low latitude. Matsumoto et al. (2002) proposed that a Silicic Acid Leakage Hypothesis

606   (SALH) could explain the drop of atmospheric pCO_2 during glacial times and would be

607   mainly driven by changes in Si:N ratios of diatoms induced by an increase in iron supply to

608   the Southern Ocean. This hypothesis is based on *in vitro* and artificial Fe-enrichment

609   experiments showing lower Si:N uptake ratios for diatoms in non Fe-stressed conditions

610   (Takeda, 1998; Hutchins & Bruland, 1998), so that the increase of Fe-deposition in the

611   Southern Ocean during glacial times would drive AASW towards NO_3^- depletion instead of

612   the actual H_4SiO_4 depletion (Brzezinski et al., 2002).

613   Our results could indicate that glacial Fe fertilization may not have necessarily resulted in a

614   decrease in Si:N uptake ratios in AASW contrary to what has been proposed as an explanation

615   for the SALH (Brzezinski et al. 2002). Other processes leading to SALH could be invoked,

616   such as shifts in AAIW and SAMW formation rates (Crosta et al., 2007), variations in

617   phytoplankton assemblages (including relative contribution of non-siliceous organisms) or

618   changes in NO_3^- remineralization efficiency. Since this interpretation is based on several

619   incubations for several samplings (during spring and summer) in a single Fe-enriched station

620   (A3, n = 4) and only one station in the HNLC region (R), further investigations concerning

621   the seasonality of net silica production and Si:N uptake ratios in both naturally Fe-fertilized

622   and HNLC areas of the Southern Ocean are clearly needed to validate this observation.

623   **4.3   Seasonality and budget of the silicon cycle above the Kerguelen Plateau**

624   In order to investigate the seasonal evolution of Si biogeochemical cycle in the Kerguelen

625   iron-fertilized bloom (station A3), we combined in figure 7 the KEOPS-1 and KEOPS-2

626   silicon fluxes measured using different isotopic approaches (stable and radiogenic isotope

627   tracer incubations: ^{30}Si and ^{32}Si respectively, and, natural silicon isotopic composition, $\delta^{30}Si$,

628   of both diatoms and seawater). Assuming that the whole water mass above the Kerguelen

629   Plateau may have been significantly ventilated with surface waters from the HNLC area at the

630   annual scale, Fripiat et al. (2011a) used the HNLC winter water (WW) characteristics to

631   represent the initial conditions of the winter H_4SiO_4 stock in the fertilized area surface layer

632   (0-100 m). Because the biological activity (Si and C assimilation) took place only in the upper

633   80 m during KEOPS-2, Si fluxes, stocks and values estimated by Fripiat et al (2011a)

634   discussed in this section were recalculated from the surface to 80 m (instead of 100 m in

635   Fripiat et al. 2011a). The winter supply of DSi estimated from the seasonal H_4SiO_4 depletion

636   during KEOPS-1 from the Upper Deep Circumpolar Water (UDCW) to the WW is around 2

637   mol m^{-2}, which is not significantly different from the 1.9 mol m^{-2} DSi stock we measured by

638   mid-October during KEOPS-2 (1st visit at A3). This confirms that, as suggested by Fripiat et

639   al (2011a), the HNLC winter water is representative of the Si source with initial Si pool

640   conditions prevailing before the bloom onset in the fertilized area. At this time, silica

641   production (which was not measured during this 1st visit) should be very low since only little

642   BSi accumulation was observed in the ML (79.1 mmol m^{-2}), and only 2 - 1.9 = 0.1 mol m^{-2} of

643   H$_4$SiO$_4$ was consumed in the surface water before our sampling compared to the estimated

644   WW initial stock. The system was likely exclusively driven by regenerated silica production

645   inducing a potentially high ∫D:∫P ratio (close to 1). Irradiance and mixed layer regime should

646   be the more likely dominant factors controlling the bloom development for eukaryotes in

647   winter and in early spring (Boyd et al., 2001; Blain et al., 2013). Models have previously

648   reported that the interannual variability of mixed layer depth significantly affects both the date

649   of the bloom onset and the maximum chlorophyll concentration in the region (Pondaven et al.,

650   1998). Then, because H$_4$SiO$_4$ and Fe were not at limiting concentrations in the surface layer

651   (Sarthou et al., in prep.), the light-mixing regime that occurred above the Plateau by mid-

652   October, should have been still unfavourable to diatom growth.

653   As the surface irradiance becomes more favourable with time, biogenic silica production

654   progressively increases and reaches the highest net production value (46.8 mmol m^{-2} d^{-1})

655   measured during our 2nd visit to A3 (mid-November). Between these 2 samplings (i.e. during

656   28 days), the H$_4$SiO$_4$ depletion in the ML (1.9 - 1.5 = 0.4 mol m^{-2}) yields to an average ∫ρNet

657   of 14.3 mmol m^{-2} d^{-1}. Although it was located in different blooms of the Kerguelen region

658   with different diatom communities, this value is in good agreement with the net silica

659   production measured at station E1 which we characterized as a "starting-bloom" dynamic.

660   Consequently, we can predict that simultaneously to the rise of silica production above the

661   Plateau, the ∫D:∫P ratio should decrease toward values around 0.5 as measured at E1, and that

662   the silica production could be controlled by both new and regenerated sources of H$_4$SiO$_4$. In

663   this situation, almost all the net BSi production is accumulated in the surface water: 348.5

664   mmol m^{-2} (BSi stock integrated over 80 m, this study) and very low export of biogenic silica

665   is allowed from the ML to the bottom layer: 4.7 mmol m^{-2} d^{-1} (estimated from the difference

666   between net production calculated with DSi standing stocks and that calculated using BSi

667   standing stocks, 14.3 and 9.6 mmol m^{-2} d^{-1} respectively). These observations are in good

668   agreement with the low carbon export (4 % of the surface primary production) estimated

669   during the first visit at A3 by Jacquet et al. (2014). Indeed, such early spring bloom generally

670   starts by the development of lightly silicified diatoms with potentially low sedimentation rates

671   (Quéguiner, 2013).

672   The H$_4$SiO$_4$ stock measured during the second visit at A3 (1.5 mol m^{-2}) can sustain the strong

673   net silica production rates measured there for 32 days. Using natural Si isotopic approach,

674   Fripiat et al. (2011a) suggested that diatoms could receive in addition, at least 1.2 mol m^{-2} of

675   DSi coming from the WW during the productive period in the upper 80 m of the fertilized

676   area, allowing 26 supplementary days of growth for diatoms with the same high Si uptake

677   rate. Taking into account the sum of such winter and summer vertical Si supply, the high

678   productive period as measured in A3 can be maintained during 86 days. Remarkably, this is

679   almost similar to the estimation by Mongin et al. (2008) based on satellite products of 85 days

680   of blooming over the Kerguelen plateau. Using a box-model approach, De Brauwere et al.

681   (2012) suggested that the bloom could also persist over the same duration without considering

682   this summer Si supply from deep-waters. This appears unlikely because the high net silica

683   production we measured at A3 could not be sustained for more than 32 days. Even if such

684   high net silica production should probably not be representative of the Si uptake by diatoms

685   over the Plateau during the rest of bloom period, an additional source of Si is needed. The

686   very good accordance of our results with the bloom duration from Mongin et al. (2008)

687   suggests that this summer H_4SiO_4 input in the ML is realistic and could sustain a significant

688   part of the phytoplankton growth above the Kerguelen Plateau. Indeed, high internal wave

689   activity above the plateau is assumed to be a major process for vertical dissolved iron (and

690   other nutrients) supply on the upper waters (Park et al., 2008; Blain et al., 2008).

691   These vertical fluxes allow a 2-month period of highly active blooming, with a system

692   controlled exclusively by new sources of H_4SiO_4 ($\int D{:}\int P = 0.09$, A3, table 3), inducing the

693   strong DSi depletion observed in January (DSi stocks at 0.2 mol m^{-2}, KEOPS-1; Mosseri et

694   al., 2008) and the high BSi accumulation in the ML (348.5 mmol m^{-2}, KEOPS-2; this study)

695   which could be exported at the end of summer when the water column stratification becomes

696   weaker. The gross-$\int\rho$Si measured here is in the upper range of published values in the

697   Southern Ocean and the specific Si uptake rate was relatively high (respectively 47.9 mmol m^{-}

698   ^{2} d^{-1} and 0.28 d^{-1} in the euphotic layer; table 2). This could indicate that diatoms have already

699   reached their maximum BSi production rate, and that our second visit to A3 could represent

700   the maximum of the bloom dynamic above the Plateau. This is quite consistent with the date

701   of the bloom peak estimated in early December both by modeling and satellite approaches

702   (Mongin et al., 2008 and de Brauwere et al., 2012). The H_4SiO_4 standing stock in the ML

703   would then be depleted by mid-January (0.2 mol m^{-2}, KEOPS-1; Mosseri et al., 2008). Then

704   the bloom would shift toward a steady state dynamic, almost entirely controlled by

705   regenerated Si with decreasing gross silica production down to 10.7 mmol m^{-2} d^{-1}, KEOPS-1

706   (Mosseri et al., 2008) and where H_4SiO_4 concentration in the ML becomes limiting for diatom

707   growth.

708   This progression of Si limitation could be associated to a change in the phytoplankton

709   community as observed between the different visits at A3 during KEOPS-1 (Mosseri et al.,

710   2008; Armand et al., 2008), and could be related to the selection of species with higher

711   affinities with silicic acid resulting in a better ability to grow at low H_4SiO_4 concentrations.

712   Such change in the community structure in response to physical and biological forcing was

713   also proposed in a conceptual scheme by Quéguiner (2013). In spring, diatoms presenting

714   high growth rates and low degree of silicification dominate the bloom which development is

715   mainly controlled by new nutrients sources. This diatom assemblage will be soon affected by

716   the availability of both silicic acid and iron, and will change for a population showing lower

717   growth rates exclusively sustained by regenerated sources of H_4SiO_4. This second

718   assemblage, beginning to dominate in January, could thus persist at steady state until May,

719   when PAR decreases below the threshold of 1 mol photon m^{-2} d^{-1} (Blain et al., 2013) in waters

720   that are quite depleted in H_4SiO_4, as it is composed by small diatoms with high affinities for

721   silicic acid (Mosseri et al., 2008) and a deep silica maximum (DSM) characterized by strongly

722   silicified large–sized diatoms growing at the base of the ML in the nutrient gradient

723   (Quéguiner, 2013). Under such conditions, a very low net silica production and a ∫D:∫P ratio

724   close to 1 are expected. Unfortunately no silica dissolution measurements are available from

725   KEOPS-1. However, we can try to estimate the net production from the difference between

726   the KEOPS-1 average gross silica production (10.7 mmol m^{-2} d^{-1}; Mosseri et al., 2008) and

727   average silica dissolution measured at all stations south of the Polar Front during KEOPS-2

728   (10.2 mmol m^{-2} d^{-1}). The choice of a constant silica dissolution rate throughout the productive

729   season may seem surprising at first sight. However, there are several reasons to support this

730   hypothesis: (i) Brzezinski et al. (2001) show that the seasonal variability of silica dissolution

731   rates in the Southern Ocean is very low (6.7 mmol m^{-2} d^{-1} in October/November to 6.6 mmol

732   m^{-2} d^{-1} in February/March); (ii) ∫ρDiss measured close to the Polar Front by Fripiat et al.

733   (2011b) in late summer were very close to our spring dissolution values (4.9 to 6.6 mmol m^{-2}

734   d^{-1}) (iii) As best seen on Fig. 4b, all KEOPS-2 stations except the HNLC one (R) have similar

735   silica dissolution profiles. Thus it is reasonable to assume that the net silica production

736   estimated above the plateau in late summer should be around 0.5 mmol m^{-2} d^{-1}.

737   The BSi standing stock observed in the upper layer in late summer (275.3 mmol m^{-2}, KEOPS-

738   1; Mosseri et al., 2008) is lower than that measured in spring (348.5 mmol m^{-2}). This could

739   indicate that a part of the BSi that was produced before reaching a silica production in steady

740   state (i.e. sustained almost entirely by regenerating production) was not accumulated in the

741   surface ML at the end of the productive period. In fact, a part of the summer production can

742   be stocked in the form a DSM as measured in late summer above the plateau (550.1 mmol m^{-2}

743   between 100 and 200 m; Mosseri et al., 2008) which was not yet present at KEOPS-2. This

744   subsurface biogenic silica accumulation mainly results from the combination of sedimentation

745   of living but inactive cells and the occurrence of phytoplankton populations living at depth

746   (Uitz et al., 2009; Fripiat et al., 2011a). The part of the summer net silica production which is

747   not accumulated below the ML should thus be exported to deeper waters as the seasonal

748   stratification breaks down with the intensification of vertical mixing. In term of carbon export,

749   this flux could represent 14 to 31 % of the surface primary production (KEOPS-1, station A3;

750   Jacquet et al., 2008). As proposed by Quéguiner (2013), a massive export of biogenic silica

751   and organic matter (58 days x 46.8 mmol m^{-2} d^{-1} - (275.3 + 550 mmol m^{-2}) = 2.2 mol Si m^{-2})

752   should occur and could then represent the major annual event of the silicon and biological

753   carbon pumps.

754   Although our budget of the silicon biogeochemical cycle above the Kerguelen Plateau is

755   based on different silicon isotopic approaches and is sustained by silicon stocks and fluxes

756   coming from different years, it matches very well with all the previous individual findings.

757   The seasonal variations of ∫D:∫P ratio are in accordance with those observed by Brzezinski et

758   al. (2001) across the Polar Front Zone and are quite well represented by the recent model of

759   Coffineau et al. (2013), who estimate a ∫D:P ratio ranging from 0.64 in winter to 0.19 during

760   the spring bloom. The good accordance of our approach with outcomes from different studies

761   also highlights that, to fully characterize the silicon cycle in a region of interest, we need to

762   measure both silica production and dissolution rates. Indeed, taking only into account the

763   gross silica production in such a synthesis exercise (i.e. without measuring silica dissolution

764   as it is the case in most studies) could lead to misinterpretations of the silicon pump

765   functioning. For instance, we would not be able to identify shifts between "new" and

766   "regenerated" silica production neither to accurately calculate the real bloom duration without

767   considering silica recycling. Without taking into account dissolution, silica production would

768   have been overestimated by 21 % in the mixed layer (58.2 mmol m^{-2} d^{-1} compared to the 47.9

769   mmol m^{-2} d^{-1} of real net silica production), and the bloom duration computation would have

770   yielded 74 days, which is not consistent with the 85 days of KEOPS-1 bloom duration

771   observed by Mongin et al. (2008).

772

5   Conclusions

Our study addressed the seasonal evolution of the efficiency of the silicon pump and of the biogenic silica fluxes in the mixed layer under different naturally iron-fertilized bloom conditions around the Kerguelen region. Integrated Si uptake rates were among the highest reported so far in the Southern Ocean. They varied from 3.09 ± 0.01 mmol m^{-2} d^{-1} in the HNLC area (R) to 47.9 ± 0.4 mmol m^{-2} d^{-1} above the plateau (A3) and seemed to be strongly coupled with C uptake over depth. Indeed, C and Si assimilation were very low below the euphotic layer indicating the occurrence of a subsurface accumulation of living but inactive diatoms. Although significant, silica dissolution rates were generally much lower than production rates and did not vary between bloom stations nor over depth.

We observed a shift from a BSi production regime based on the regeneration of H_4SiO_4 during the early stages of bloom onset (with an averaged $\int D$:$\int P$ ratio of 0.98) to a regime based on new production during the bloom development (with an averaged $\int D$:$\int P$ ratio of 0.18). This change switched on an active silicon pump which led to the decoupling between Si and N cycles as well as a strong H_4SiO_4 depletion of surface water by late summer, with significant implications for global biogeochemical properties. Indeed, the system progressively shifted toward a stronger silicon pump as Si uptake rates increased and nitrogen became preferentially remineralized when the bloom was well established. This led ultimately to a strong Si limitation and drove the system toward a regenerated silica production regime which allowed the persistence of the bloom in a steady state despite the low concentrations of silicic acid concentrations. Our results confirm and complete the concept of a seasonal transition from a diatom new production to a diatom regenerated production already proposed in the Antarctic Zone by Brzezinski et al. (2003).

Moreover, in opposition to previous artificial Fe-enrichment bottle experiments outcomes, Si:N and Si:C uptake ratios during KEOPS-2 were not higher in the HNLC area compared to the fertilized region. This observation could have great implications on our understanding on processes involved in setting atmospheric pCO$_2$ during glacial-interglacial transitions. Our results suggest that the increase of low latitude diatom production observed during glacial periods should not be controlled primarily by a shift in the nutrient uptake stoichiometry of Antarctic diatoms induced by an enhanced iron supply, as proposed in the silicic acid leakage hypothesis (Matsumoto et al., 2002; Brzezinski et al., 2002), but further investigations are clearly needed to validate this idea.

805   The combination of the results from the two KEOPS cruises (early spring and late summer)

806   and of different isotopic approaches, allowed the first seasonal estimate of a closed silicon

807   biogeochemical budget in the iron-fertilized area above the Kerguelen Plateau based on direct

808   measurements. Our estimates emphasize the interest of combining different tracers and

809   methods with different sensitivities to physical and biological processes to better constrain

810   and quantify all the processes simultaneously. The major outcome of this seasonal budget is

811   that the winter and summer silicon supplies to the mixed layer (3.2 mol m^{-2} y^{-1}) seem to be

812   well balanced by the combination of biogenic silica accumulation (both in the upper layer and

813   in the winter waters) and late summer BSi export (respectively $0.3 + 0.6 + 2.2 = 3.1$ mol m^{-2}

814   y^{-1}). This confirms the occurrence of a significant summer Si supply from Winter Water as

815   suggested by Fripiat et al. (2011a) sustaining the diatom bloom over the Kerguelen Plateau.

816   Finally, a striking feature of this study is that naturally iron fertilized areas of the Southern

817   Ocean, like the Kerguelen Plateau, could sustain a biogenic silica production regime similar to

818   those observed in coastal upwelling systems or in large river plume. This highlights the

819   exceptional character of diatoms-dominated ecosystems associated to natural iron fertilization

820   in the Southern Ocean, and their significant role in the global Si biogeochemical cycle. Even

821   if the outcomes of this budget are consistent with previous measurements, large uncertainties

822   remain about the seasonal evolution of dissolution rates at the end of the productive period.

823   Indeed, in order to fully characterize the Si-biogeochemical cycle in a region of interest, it is

824   recommended to measure both BSi production and dissolution rates. In combination, the

825   natural silicon isotopic composition (δ^{30}Si) of diatoms and seawater represents a powerful tool

826   for identifying silicon sources and silica production over larger temporal and spatial scales

827   (Fripiat et al., 2011a; Tréguer and De la Rocha, 2013), and will be also examined during

828   KEOPS-2. The combination of several isotopic approaches, as well as modeling exercises

829   (such as in Pondaven et al., 1998; De Brauwere et al., 2012; Coffineau et al., 2013), by

830   allowing to better constrain and quantify different physical and biogeochemical processes

831   simultaneously, would strongly improve our understanding of the regional Si biogeochemical

832   cycle and its implications in the global ocean biogeochemistry.

833

846

References

848 Assmy P., Smetacek V., Montresor M., Klaas C., Henjes J., Strass V., Arrieta J., Bathmann

849 U., Berg G., Breitbarth E., Cisewski B., Friedrichs L., Fuchs N., Herndl G., Jansen S.,

850 Krägefsky S., Latasa M., Peeken I., Röttgers R., Scharek R., Schüller S., Steigenberger S.,

851 Webb A., Wolf-Gladrow D.: Thick-shelled, grazer-protected diatoms decouple ocean carbon

852 and silicon cycles in the iron-limited Antarctic Circumpolar Current. Proceedings of the

853 National Academy of Sciences of the United States of America. 110(51):20633–20638, 2013.

854 Armand L., Cornet-Barthaux V., Mosseri J., Quéguiner B.: Late summer diatom biomass and

855 community structure on and around the naturally iron-fertilised Kerguelen Plateau in the

856 Southern Ocean. Deep-Sea Research II. 55:653-676, 2008.

857 Baines S., Twining B., Brzezinski M., Nelson D., Fisher N.: Causes and biogeochemical

858 implications of regional differences in silicification of marine diatoms. Global

859 Biogeochemical Cycles. 24:GB4031. Doi10.1029/2010GB003856, 2010.

860 Beucher C., Tréguer P., Hapette A. M., Corvaisier R.: Intense summer Si-recycling in the

861 surface Southern Ocean. Geophysical research letters. 31:L09305.

862 doi:10.1029/2003GL018998, 2004.

863 Bidle K. D., Azam F.: Accelerated dissolution of diatom silica by marine bacterial

864 assemblages. Nature. 397:508-512, 1999.

865   Bidle K. D., Brzezinski M., Long R., Jones J., Azam F.: Diminished efficiency in the oceanic
866   silica pump caused by bacteria-mediated silica dissolution. Limnology and Oceanography.
867   48(5):1855-1868, 2003.

868   Blain S., Tréguer P., Belviso S., Bucciarelli E., Denis M., Desabre S., Fiala M., Martin-
869   Jézéquel V., Le Fèvre J., Mayzaud P., Marty J.-C., Razouls S.: A biogeochemical study of the
870   island mass effect in the context of the iron hypothesis: Kerguelen Islands, Southern Ocean.
871   Deep-Sea Research I. 48:163-187, 2001.

872   Blain S., Quéguiner B., Armand L., Belviso S., Bombled B., Bopp L., Bowie A., Brunet C.,
873   Brussaard C., Carlotti F., Christaki U., Cordière A., Durand I., Ebersbach F., Fuda J.-L.,
874   Garcia N., Gerringa L., Griffiths B., Guigue C., Guillerm C., Jacquet S., Jeandel C., Laan P.,
875   Lefèvre D., Lo Monaco C., Malits A., Mosseri J., Obernosterer I., Park Y.-H., Picheral M.,
876   Pondaven P., Remenyi T., Sandroni V., Sarthou G., Savoye N., Scouarnec L., Souhaut M.,
877   Thuiller D., Timmermans K., Trull T., Uitz J., Van Beek P., Velhuis M., Vincent D., Viollier
878   E., Vong L., Wagener T.: Effect of natural iron fertilization on carbon sequestration in the
879   Southern Ocean. Nature. 446:1070-1075, 2007.Boyd P., Crossley A., diTullio G., Friffiths F.,
880   Hutchins D., Queguiner B., Sedwick P., Trull T.: Control of phytoplankton growth by iron
881   supply and irradiance in the subantarctic Southern Ocean: Experimental results from the SAZ
882   Project. Journal of Geaophysical Research. 106:31573-31583, 2007.

883   Blain S., Quéguiner B., Trull T.: The natural iron fertilization experiment KEOPS (KErguelen
884   Ocean and Plateau compared Study): An overview. Deep-Sea Research II. 55:559-565, 2008.

885   Blain S., Renaut S., Xing X., Claustre H., Guinet C.: Instrumented elephant seals reveal the
886   seasonality in chloropyll and light-mixing regime in the iron fertilized Southern Ocean.
887   Geophysical Research Letters. 40:1-5, 2013.

888   Blain S.: KEOPS2: implementation and overview. In preparation for Biogeosciences.

889   Boyd P., Crossley A., DiTullio G., Griffiths F., Hutchins D., Quéguiner B., Sedwick ., Trull
890   T.: Control of phytoplankton growth by iron supply and irradiance in the subantarctic
891   Southern Ocean: Experimental results from the SAZ Project. Journal of Geophysical
892   Research. 106(C12):31573-31583, 2001.

893   Boyd P., Jickells T., Law C., Blain S., Boyle E., Buesseler K., Coale K., Kullen J., De Baar
894   H., Follows M., Harvey M., Lancelot C., Levasseur M., Owens N., Pollard R., Rivkin R.,

895   Sarmiento J., Schoemann V., Smetacek V., Takeda S., Tsuda A., Turner S., Watson A.:

896   Mesoscale Iron Enrichment Experiments 1993-2005: Synthesis and Future Directions.

897   Science. 315:612-617, 2007.

898   Brzezinski M.: The Si:C:N ratio of marine diatoms: interspecific variability and the effect of

899   some environmental variables. Journal of Phycology. 21:347-357, 1985.

900   Brzezinski M., Nelson D.: Seasonal changes in the silicon cycle within a Gulf Stream warm-

901   core ring. Deep-Sea Research. 36(7):1009-1030, 1989.

902   Brzezinski M., Nelson D., Franck V., Sigmon D.: Silicon dynamics within an intense open-

903   ocean diatom bloom in the Pacific sector of the Southern Ocean. Deep-Sea Research II.

904   48:3997-4018, 2001.

905   Brzezinski M. A., Pride C. J., Frank V. M., Sigman D. M., Sarmiento J. L., Matsumoto K.,

906   Gruber N., Rau G. H., Coale K. H.: A switch from $Si(OH)_4$ to NO_3^- depletion on the glacial

907   Southern Ocean. Geophysical Research Letters. 29(12), doi:10.1029/2001GL014349, 2002.

908   Brzezinski M., Jones J., Bidle K., Azam F.: The balance between silica production and silica

909   dissolution in the sea: Insights from Monterey Bay, California, applied to the global data set.

910   Limnology and Oceanography. 48(5):1846-1854, 2003.

911   Bucciarelli E., Pondaven P., Sarthou G.: Effects of an iron-light co-limitation on the elemental

912   composition (Si, C, N) of the marine diatoms Thalassiosira oceanica and Ditylum brightwellii.

913   Biogeosciences. 7:657-669, 2010.

914   Buesseler K., Ball L., Andrews J., Cochran J., Hirschberg D., Bacon M., Fleer A., Brzezinski

915   M.: Upper ocean export of particulate organic carbon and biogenic silica in the Southern

916   Ocean along 170°W. Deep-Sea Research II. 48:4275-4297, 2001.

917   Cavagna A. J. Blain S., Cardinal D., Closset I., Dehairs F., Fernandez C., Flores-Leive L.,

918   Lasbleiz M., Lefèvre D., Leblanc K., Quéguiner B.: Biological productivity regime and in-situ

919   methods comparison around the Kerguelen Island in the Southern Ocean. KEOPS 2 primary

920   and community producers regime using various uptake rates and their stoichiometric ratios. In

921   preparation for Biogeosciences.

922   Claquin P., Martin-Jézéquel V., Kromkamp J. C., Veldhuis M. J. W., Kraay G. W.:

923   Uncoupling of silicon compared to carbon and nitrogen metabolisms, and role of the cell

924   cycle, in continuous cultures of Thalassiosira pseudonana (Bacillariophyceae) under light,

925   nitrogen and phosphorus control. Journal of Phycology. 38:922-930, 2002.

926   Coffineau N., De La Rocha C., Pondaven P.: Exploring interacting influences on the silicon

927   isotopic composition of the surface ocean: a case study from the Kerguelen Plateau.

928   Biogeosciences Discussion. 10:11405-11446, 2013.

929   Corvaisier R., Tréguer P., Beucher C., Elskens M.: Determination of the rate of production

930   and dissolution of biosilica in marine waters by thermal ionisation mass spectrometry.

931   Analytica Chimica Acta. 534:149-155, 2005.

932   Crosta X., Beucher C., Pahnke K., Brzezinski M.: Silicic acid leakage from the Southern

933   Ocean: Opposing effects of nutrient uptake and oceanic circulation. Geophysical Research

934   Letters. 34, L13601, doi:10.1029/2006GL029083, 2007.

935   De Baar H., Boyd P., Coale K., Landry M., Tsuda A., Assmy P., Bakker D., Bozec Y., Barber

936   R., Brzezinski M., Buesseler K., Boye M., Croot P., Gervais F., Gorbunov M., Harrison P.,

937   Hiscock W., LaanP., Lancelot C., Law C., Levasseur M., Marchetti A., Millero F., Nishioka

938   J., Nojiri Y., van Oijen T., Riebesell U., Rikenberg M., Saito H., Takeda S., Timmermans K.,

939   Veldhuis M., Waite A., Wong C.-S.: Synthesis of iron fertilization experiments: From the Iron

940   Age in the Age of Enlightenment. Journal of Geophysical Research. 110:C09S16,

941   doi:10.1029/2004JC002601, 2005.

942   De Brauwere A., De Ridder F., Elskens M., Schoukens J., Pintelon R., Baeyens W.: Refined

943   parameter and uncertainty estimation when both variables are subject to error. Case study:

944   estimation of Si consumption and regeneration rates in a marine environment. Journal of

945   Marine Systems. 55:205-221, 2005.

946   De Brauwere A., Fripiat F., Cardinal D., Cavagna A.-J., De Ridder F., André L., Elskens M.:

947   Isotopic model of oceanic silicon cycling: the Kerguelen Plateau case study. Deep-Sea

948   Research I. 70:42-59, 2012.

949   Dehairs F., Trull T., Fernandez C., Davies D., Cavagna A. J., Planchon F., Fripiat F.: Nitrate

950   isotopic composition in the Kerguelen area (Southern Ocean) during KEOPS 2. In preparation

951   for Biogeosciences.

952   Dugdale R., Wilkerson F., Minas H.: The role of a silicate pump in driving new production.

953   Deep-Sea Research I. 5(42):697-719, 1995.

954   Elskens M., de Brauwere A., Beucher C., Corvaisier R., Savoye N., Tréguer P., Baeyens W.:

955   Statistical process control in assessing production and dissolution rates of biogenic silica in

956   marine environments. Marine Chemistry. 106:272-286, 2007.

957   Franck V., Brzezinski M., Coale K., Nelson D.: Iron and silicic acid concentrations regulate

958   Si uptake north and south of the Polar Frontal Zone in the Pacific Sector of the Southern

959   Ocean. Deep-Sea Research II. 47:3315-3338, 2000.

960   Fripiat F., Corvaisier R., Navez J., Elskens M., Schoemann V., Leblanc K., André L.,

961   Cardinal D.: Measuring production-dissolution rates of marine biogenic silica by ^{30}Si-isotope

962   dilution using a high-resolution sector field inductively coupled plasma mass spectrometer.

963   Limnology and Oceanography: Methods. 7:470-478, 2009.

964   Fripiat F.: Isotopic approaches of the silicon cycle: The Southern Ocean case study (Ph. D.

965   dissertation). Université Libre de Bruxelles, Brussels. 266p. 2010.

966   Fripiat F., Cavagna A. J., Savoye N., Dehairs F., André L., Cardinal D.: Isotopic constraints

967   on the Si-biogeochemical cycle of the Antarctic Zone in the Kerguelen area (KEOPS). Marine

968   Chemistry. 123:11-22, 2011a.

969   Fripiat F., Leblanc K., Elskens M., Cavagna A. J., Armand L., André L., Dehairs F., Cardinal

970   D.: Efficient silicon recycling in summer in both the Polar Frontal and Subantarctic Zones of

971   the Southern Ocean. Marine Ecology Progress Series. 435:47-61, 2011b.

972   Hildebrand M.: Diatoms, Biomineralization Processes, and Genomics. Chemical Review.

973   108(11):4855-4874, 2008.

974   Hutchins D., Bruland K.: Iron-limited diatom growth and Si:N uptake ratios in a coastal

975   upwelling regime. Nature. 393:561-564, 1998.

976   Jacquet S. H. M., Dehairs F., Savoye N., Obernosterer I., Christaki U., Monnin C., Cardinal

977   D.: Mesopelagic organic carbon remineralization in the Kerguelen Plateau region tracked by

978   biogenic particulate Ba. Deep-Sea Research II. 55:868-879, 2008.

979   Jacquet S. H. M., Dehairs F., Cavagna A. J., Planchon F., Monin L., André L., Closset I.,
980   Cardinal D.: Early season mesopelagic carbon remineralization and transfer efficiency in the
981   naturally iron-fertilized Kerguenlen area. Biogeosciences Discussion. 11:9035-9069, 2014.

982   Kamatani A.: Dissolution rates of silica from diatoms decomposing at various temperatures.
983   Marine Biology. 68:91-96, 1982.

984   Karl D., Tien G.: MAGIC: A sensitive and precise method for measuring dissolved
985   phosphorus in aquatic environment. Limnology and Oceanography. 37(1):105-116, 1992.

986   Krause J. W., Nelson D. M., Brzezinski M. A.: Biogenic silica production and the diatom
987   contribution to primary production and nitrate uptake in the eastern equatorial Pacific Ocean.
988   Deep-Sea Research II. 58:434-448, 2011

989   Lasbleiz M., Leblanc K., Blain S., Ras J., Cornet-Barthaux V., Hélias Nunige S., Quéguiner
990   B.: Pigments, elemental composition (C, N, P, Si) and stoichiometry of particulate matter, in
991   the naturally iron fertilized region of Kerguelen in the Southern Ocean. Biogeosciences
992   Discussion. 11:8259-8324.

993   Leynaert A., Bucciarelli E., Claquin P., Dugdale R. C., Martin-Jézéquel V., Pondaven P.,
994   Ragueneau O.: Effect of iron deficiency on diatom cell size and silicic acid uptake kinetics.
995   Limnology and Oceanography. 49(4):1134-1143, 2004.

996   Matsumoto K., Sarmiento J. L., Brzezinski M. A.: Silicic acid leakage from the Southern
997   Ocean: A possible explanation for glacial atmospheric pCO2. Global Biogeochemical Cycles.
998   16(3), doi:10.1029/2001GB001442, 2002

999   Martin-Jézéquel V., Hildebrand M., Brzezinski M.: Silicon metabolism in diatoms:
1000 implications for growth. Journal of Phycology. 36:821-840, 2000.

1001 Mongin M., Molina E., Trull T.: Seasonality and scale of the Kerguelen plateau
1002 phytoplankton bloom: A remote sensing and modeling analysis of the influence of natural iron
1003 fertilization in the Southern Ocean. Deep-Sea Research II. 55:880-892, 2008.

1004 Mosseri J., Quéguiner B., Armand L., Cornet-Barthaux V.: Impact of iron on silicon
1005 utilization by diatoms in the Southern Ocean: A case study of Si/N cycle decoupling in a
1006 naturally iron-enriched area. Deep-Sea Research II. 55:810-819, 2008.

1007   Nelson D. and Goering J. J.: A Stable Isotope Tracer Method to Measure Silicic Acid Uptake

1008   by Marine Phytoplankton. Analytical Biogeochemistry. 78:139-147, 1977a.

1009   Nelson D. and Goering J. J.: Near-surface silica dissolution in the upwelling region off

1010   northwest Africa. Deep –Sea Research. 24:65-73, 1977b.

1011   Nelson D., Tréguer P.: Role of silicon as a limiting nutrient to Antarctic diatoms: evidence

1012   from kinetic studies in the Ross Sea ice-edge zone. Marine ecology progress series. 80:255-

1013   264, 1992.

1014   Park Y.-H., Charriaud E., Ruiz Pino D., Jeandel C.: Seasonal and interannual variability of the

1015   mixed layer properties and steric height at station KERFIX, southwest of Kerguelen. Journal

1016   of Marine Systems. 17:571-586, 1998.

1017   Park Y.-H., Roquet F., Durand I., Fuda J.-L.: Large-scale circulation over and around the

1018   Northern Kerguelen Plateau. Deep-Sea Research II. 55:566-581, 2008.

1019   Park Y.-H.: Water masses and circulation in the Polar Front region east of the Kerguelen

1020   Islands. In preparation for Biogeosciences.

1021   Pollard R., Lucas M., Read J.: Physical controls on biogeochemical zonation in the Southern

1022   Ocean. Deep-Sea Research II. 49:3289-3305, 2002.

1023   Pondaven P., Fravalo C., Ruiz-PinoD., Tréguer P., Quéguiner B., Jeandel C.: Modelling the

1024   silica pump in the Permanently Open Ocean Zone of the Southern Ocean. Journal of Marine

1025   Systems. 17:587-619, 1998.

1026   Pondaven P., Ragueneau O., Tréguer P., Hauvespre A., Dézileau L., Reyss J.L.: Resolving the

1027   "opal paradox" in the Southern Ocean. Nature. 405(6783):168-172, 2000.

1028   Quéguiner B.: Biogenic silica production in the Australian sector of the Subantarctic Zone of

1029   the Southern Ocean in late summer 1998. Journal of Geophysical Research. 106(C12):31627-

1030   31636, 2001.

1031   Quéguiner B.: Iron fertilization and the structure of planktonic communities in high nutrient

1032   regions of the Southern Ocean. Deep-Sea Research II. 90:43-54, 2013.

1033   Quéguiner B., Brzezinski M.: Biogenic silica production rates and particulate organic matter

1034   distribution in the Atlantic sector of the Southern Ocean during austral spring 1992. Deep-Sea

1035   Research II. 49:1765-1786, 2002.

1036   Quéroué F.: Dissolved iron in the vicinity of the Kerguelen plateau (KEOPS-2 experiment). In

1037   preparation for Biogeosciences.

1038   Ragueneau O., Treguer P., Leynaert A., Anderson R. F., Brzezinski M. A., DeMaster D. J.,

1039   Dugdale R. C., Dymont J., Fisher G., François R., Heinze C., Maier-Reimer E., Martin-

1040   Jézéquel V., Nelson D. M., Quéguiner B.: A review of the Si cycle in the modern ocean:

1041   recent progress and missing gaps in the application of biogenic opal as a paleoproductivity

1042   proxy. Global Planet Change. 26:317-365, 2000.

1043   Ragueneau O., Savoye N., Del Amo Y., Cotten J., Tardiveau B., Leynaert A.: A new method

1044   for the measurement of biogenic silica in suspended matter of coastal waters: using Si:Al

1045   ratios to correct for the mineral interference. Continental Shelf Research. 25:697-710, 2005.

1046   Reynolds B., Frank M., Halliday A.: Silicon isotope fractionation during nutrient utilization in

1047   the North Pacific. Earth and Planetary Science Letters. 244:431-443, 2006.

1048   Roquet F., Park Y.-H. Guinet C., Bailleul F., Charrassin J.-B.: Observations of the Fawn

1049   Trough Current over the Kerguelen Plateau from instrumented elephant seals. Journal of

1050   Marine Systems. 78:377-393, 2009.

1051   Sarmiento J., Gruber N., Brzezinski M., Dunne J.: High-latitude controls of thermocline

1052   nutrients and now latitude biological productivity. Nature. 427:56-60, 2004.

1053   Sarthou G., Chever F., Quéroué F., Bowie A., Van der Merwe P., Cheize M., Sirois M.,

1054   Bucciarelli E.: Fe-Cu impact in incubation experiments of natural plankton communities and

1055   Fe- and Cu-binding ligand production at the vicinity of the Kerguelen Island, Southern Ocean.

1056   In preparation for Biogeosciences.

1057   Strickland J., Parsons T.: A pratical handbook of sea water analysis. Fisheries research board

1058   of Canada. 167:65-70, 1972.

1059   Tagliabue A., Mtshali T., Aumont O., Bowie A., Klunder M., Roychoudhury A., Swart S.: A

1060   global compilation of dissolved iron measurements: focus on distributions and processes in

1061   the Southern Ocean. Biogeosciences. 9:2333-2349, 2012.

1062   Takahashi T. ,Sutherland S., Wanninkhof R., Sweeney C., Feely R., Chipman D., Hales B.,

1063   Friederich G., Chavez F., Sabine C., Watson A., Bakker E., Schuster U., Metzl N.,

1064   Yoshikawa-Inoue H., Ishii M., Midorikawa T., Nojiri Y., Körtzinger A., Steinhoff T.,

1065   Hoppema M., Olafsson J., Arnarson T., Tilbrook B., Johannessen T., Olsen A., Bellerby R.,

1066   Wong C.S., Delille B., Bates N.R., debar H.: Climatological mean and decadal change in

1067   surface ocean pCO2, and net sea-air CO2 flux over the global oceans. Deep-sea Research II.

1068   56:554-577, 2009.

1069   Takeda S.: Influence of iron availability on nutrient consumption ratio of diatoms in oceanic

1070   waters. Nature. 393:774-777, 1998.

1071   Tréguer P., De La Rocha C. : The World Ocean Silica Cycle. Annual Review of Marine

1072   Science. 5:477-501, 2013.

1073   Trull T., Rintoul S., Hadfield M., Abraham E.: Circulation and seasonal evolution of polar

1074   waters south of Australia: Implications for iron fertilization of the Southern Ocean. Deep-Sea

1075   Research II. 48:2439-2466, 2001.

1076   Uitz J., Claustre H., Griffiths B., Ras J., Garcia N., Sandroni V.: A phytoplankton class-

1077   specific primary production model applied to the Kerguelen Islands region (Southern Ocean).

1078   Deep-Sea Research I. 56:541-560, 2009.

1079   Zhou M., Zhu Y., d'Ovidio F., Park Y.-H., Durand I., Kestenare E., Sanial V., Van-Beek P.,

1080   Quéguiner B., Carlotti F., Blain S.: Surface currents and upwelling in Kerguelen Plateau

1081   regions. Biogeosciences Discussion. 11:68-6876, 2014.

1082

1083   **Tables**

1084   Table 1: Characteristics of the stations sampled for Si-fluxes measurements during KEOPS-2.

1085   Ze represents the bottom of the euphotic zone (1% of surface Photosynthetically Active

1086   Radiation), MLD is the depth of the Mixed Layer (from Park et al., in prep.).

Station	Zone	Position Latitude	Longitude	Date	Ze (m)	MLD (m)
R	*HNLC*	50°21.55 S	66°43.0 E	26-Oct	92	124
E1	*Meander*	48°27.4 S	72°11.3 E	30-Oct	64	69
E3	*Meander*	48°42.1 S	71°58.0 E	4-Nov	68	35
F	*Polar front*	48°31.2 S	74°39.5 E	7-Nov	29	47
E4W	*Plume*	48°45.9 S	71°25.5 E	12-Nov	31	55
E4E	*Meander*	48°42.9 S	72°33.8 E	14-Nov	34	80
A3	*Plateau*	50°37.5 S	72°34.9 E	17-Nov	38	123
E5	*Meander*	48°24.7 S	71°54.0 E	19-Nov	54	41

1087

1088

1089 Table 2: Biogenic silica concentration ($\int$[BSi]), Si-uptake ($\int\rho$Si), biogenic silica dissolution

1090 ($\int\rho$Diss), silica net production ($\int\rho$Net) integrated over the euphotic layer (1% of surface

1091 Photosynthetically Active Radiation), and integrated specific rates of Si-uptake and silica

1092 dissolution (calculated as $\int$VSi = $\int\rho$Si/[BSi] and $\int$Diss = $\int\rho$Diss/[BSi] respectively).

Station	Zone	$\int$[BSi] mmol m^{-2}	$\int\rho$Si mmol m^{-2} d^{-1}	$\int\rho$Diss mmol m^{-2} d^{-1}	$\int\rho$Net mmol m^{-2} d^{-1}	Specific rates $\int$VSi (d^{-1})	$\int$VDiss (d^{-1})
R	*HNLC*	33.28 ± *0.1*	3.09 ± *0.01*	4.88 ± *0.01*	-1.78 ± *0.02*	0.09	0.15
E1	*Meander*	96.1 ± *0.2*	16.8 ± *0.1*	7.11 ± *0.02*	9.6 ± *0.1*	0.17	0.07
E3	*Meander*	83.6 ± *0.2*	10.5 ± *0.1*	9.99 ± *0.03*	0.5 ± *0.1*	0.13	0.12
F	*Polar front*	97.8 ± *0.5*	27.5 ± *0.3*	3.79 ± *0.03*	23.8 ± *0.3*	0.28	0.04
E4W	*Plume*	142.0 ± *0.7*	31.8 ± *0.3*	3.97 ± *0.03*	27.9 ± *0.3*	0.22	0.03
E4E	*Meander*	104.3 ± *0.5*	21.0 ± *0.2*	5.89 ± *0.03**	15.1 ± *0.2**	0.20	0.06*
A3	*Plateau*	173.6 ± *0.7*	47.9 ± *0.4*	4.50 ± *0.03*	43.4 ± *0.4*	0.28	0.03
E5	*Meander*	159.5 ± *0.4*	27.5 ± *0.2*	6.97 ± *0.03*	20.5 ± *0.2*	0.17	0.04

1094 * Since no dissolution rates were measured at E4E, these values do not correspond to calculations from direct

1095 measurements but only to estimations. Dissolution was calculated as the average of all KEOPS-2 integrated

1096 dissolution rates.

1097

1098 Table 3.:Dissolution to production ratio ($\int$D:$\int$P), fraction of the silica production supported by

1099 new silicic acid (1-$\int$D:$\int$P), silicon to carbon (C) and nitrogen (N) uptake ratios (C and N

1100 assimilation were measured by Cavagna et al., in prep.). ρN represents both nitrate and

1101 ammonium uptake. All these values are integrated over the euphotic layer (1% of surface

1102 Photosynthetically Active Radiation).

Station	Zone	∫D:∫P	1-∫D:∫P	gross-∫ρSi:∫ρC	gross-∫ρSi:∫ρN
R	*HNLC*	1.58	-0.58	0.28	0.44
E1	*Meander*	0.42	0.58	0.38	1.27
E3	*Meander*	0.95	0.05	0.18	0.74
F	*Polar front*	0.14	0.86	0.1	0.32
E4W	*Plume*	0.12	0.88	0.15	0.93
E4E	*Meander*	0.28*	0.72*	0.27	1.26
A3	*Plateau*	0.09	0.91	0.3	1.51
E5	*Meander*	0.25	0.75	0.35	1.41

1103

1104 * Since no dissolution rates were measured at E4E, these values do not correspond to calculations from direct

1105 measurements but only to estimations. Dissolution was calculated as the average of all KEOPS-2 integrated

1106 dissolution rates.

1107

1108 **Figures captions**

1109 Figure 1: Map of the KEOPS-2 cruise area (Indian sector of the Southern Ocean) showing the

1110 location of stations discussed in this study. Dotted line represents the position of the Polar

1111 Front from Park et al. (in prep.).

1112 Figure 2. Comparison of changes in ^{30}Si-abundance of seawater for each incubation (symbols)

1113 with detection limit of the ^{30}Si-isotopic dilution method (plain line) estimated from the

1114 reproductibility of an internal standard (0.43‰, n = 40). The dotted line represents the

1115 detection limit obtained from the average reproductibility of all dissolution duplicates (0.32‰,

1116 n = 35).

1117 Figure 3: Vertical distribution of chlorophyll *a* (continuous-black line; estimated from CTD

1118 fluorescence), biogenic silica concentration ([BSi], light dots) and H_4SiO_4 concentration

1119 ([DSi], dark dots). Dotted lines show the bottom of the euphotic layer (1% of

1120 Photosynthetically Active Radiation, Ze) for each station. Dark dashed lines represent the

1121 Mixed Layer Depth (MLD; estimated by Park et al., in prep.) and grey dashed lines

1122 correspond to a 2nd density gradient identify from the density CTD-profile.

1123 Figure 4: Vertical distribution of Si-uptake (ρSi, panel a.) and biogenic silica dissolution

1124 (ρDiss, panel b.) in KEOPS-2 stations. Open symbols represent the depth at the bottom of the

1125 euphotic layer (1% of Photosynthetically Active Radiation) for each station.

1126   Figure 5: Si-uptake (black), biogenic silica dissolution (white) and net silica production (grey)

1127   integrated over the euphotic layer (1% of Photosynthetically Active Radiation). Italic values

1128   correspond to the integrated dissolution to production ratio ($\int$D:$\int$P).

1129   Figure 6: Fraction of biogenic silica production supported by new silicic acid (1-$\int$D:$\int$P) as a

1130   function of the integrated net silica production rate ($\int\rho_{net}$) during KEOPS-2 (filled black

1131   diamonds) compared with different regions of the global ocean (Open circles; Brzezinski et

1132   al., 2003 and references therein; and open diamonds; Fripiat et al., 2011b). Triangles and

1133   squares show the mean values for different growth seasons for SAZ and PFZ, respectively

1134   (Fripiat et al., 2011b). The plain line is a rectangular hyperbola to fit all data points (grey

1135   symbols were excluded from the model since they represent either negative 1-$\int$D:$\int$P value

1136   which are not allowed by the model, or average while all other symbols refer to single

1137   stations). The equation of the curve is 1-$\int$D:$\int$P = 1.01 x $\int\rho_{net}$/(5.89 + $\int\rho_{net}$). Dotted lines

1138   correspond to ± 1sd of the 1-$\int$D:$\int$P$_{max}$.

1139   Figure 7: Schematic view of the seasonal silicon cycle in the mixed layer above the Kerguelen

1140   Plateau as estimated from natural and enriched Si isotopic measurements. Blue silicon fluxes

1141   correspond to estimated values while dark fluxes correspond to direct measurements. The 3

1142   main water masses are represented by dark-grey for Upper Circumpolar Deep Water

1143   (UCDW), medium-grey for the Winter Water (WW) and light-grey for the Mixed Layer

1144   (ML). Variation of biogenic silica and H_4SiO_4 standing stocks integrated over 80m

1145   (respectively [BSi] and [DSi]) are shown in the upper panel. Vertical continuous arrows

1146   represent DSi supplies from deep water to the ML, and dotted arrows correspond to

1147   particulate silica fluxes. Integrated silica production rates are calculated from the surface to

1148   80m. Horizontal white arrows represent the state of the bloom (indicated by the D:P ratio)

1149   through time. Winter consumption has been estimated from the difference of winter mixing

1150   supply (Fripiat et al., 2011a) and the standing stock measured at the first A3 visit (KEOPS-2).

1151   The difference in standing stocks between the two visits at A3 (28 days, KEOPS-2) yields to

1152   the net silica production of 14.3 mmol.m^{-2}.d^{-1}. The DSi standing stock at the second visit of

1153   A3 can sustain the net silica production measured for 32 days (this study) while the summer

1154   DSi supply estimated by Fripiat et al. (2011a) can sustain the same net production by an extra

1155   26 days. The fall production measurements and standing stocks are from Mosseri et al. (2008,

1156   KEOPS-1). Since no silica dissolution is available from KEOPS-1, fall net production has

1157   been estimated from the difference between average gross silica production during KEOPS-1

1158 (Mosseri et al., 2008) and average silica dissolution measured at all stations south of the Polar

1159 Front (KEOPS-2, this study). Deep BSi accumulation is calculated by integrating over the

1160 100-200m depth layer data from Mosseri et al. 2008 (see text for further details).
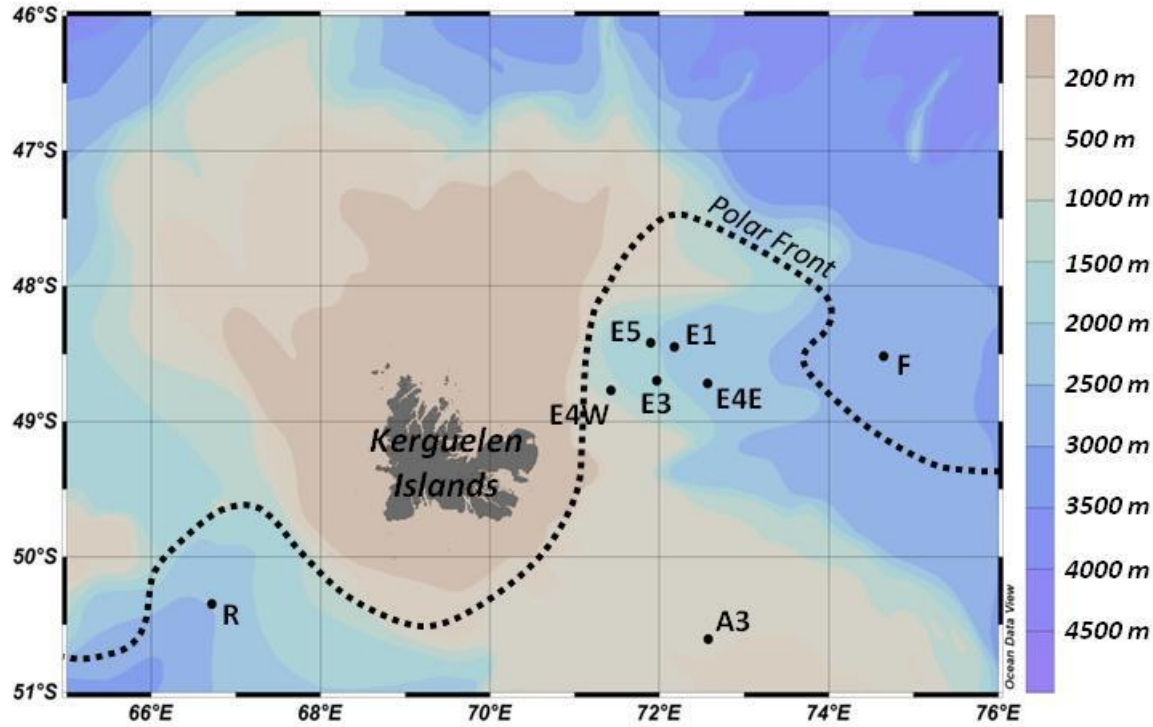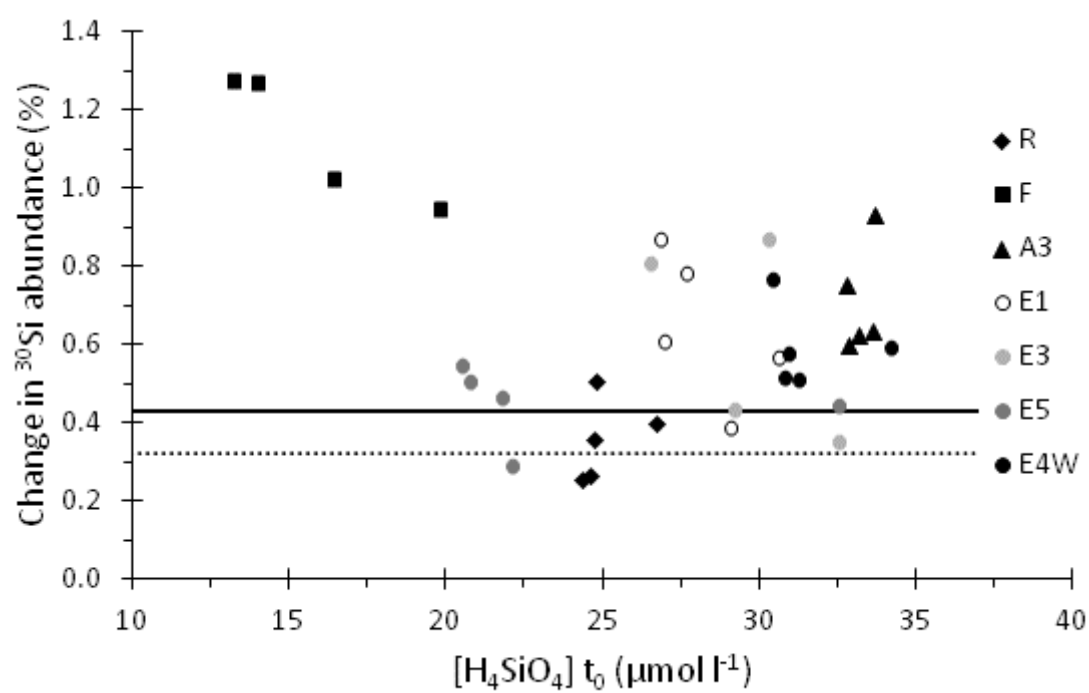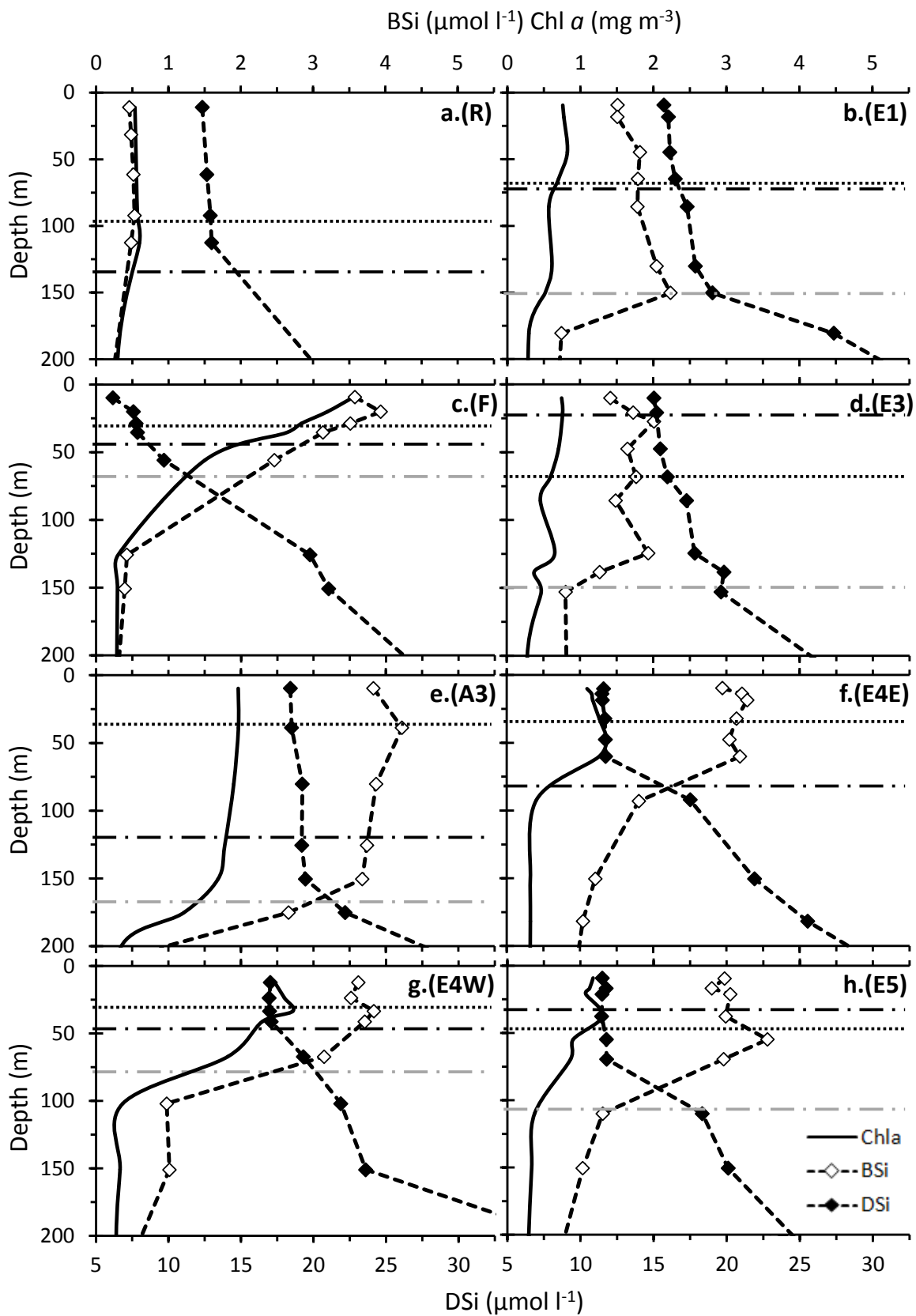
1161

1162 **Figures**

1163

1164 Figure 1.

1165

1166   Figure 2.

1167

1168   Figure 3.

1169

1170   Figure 4.

1171
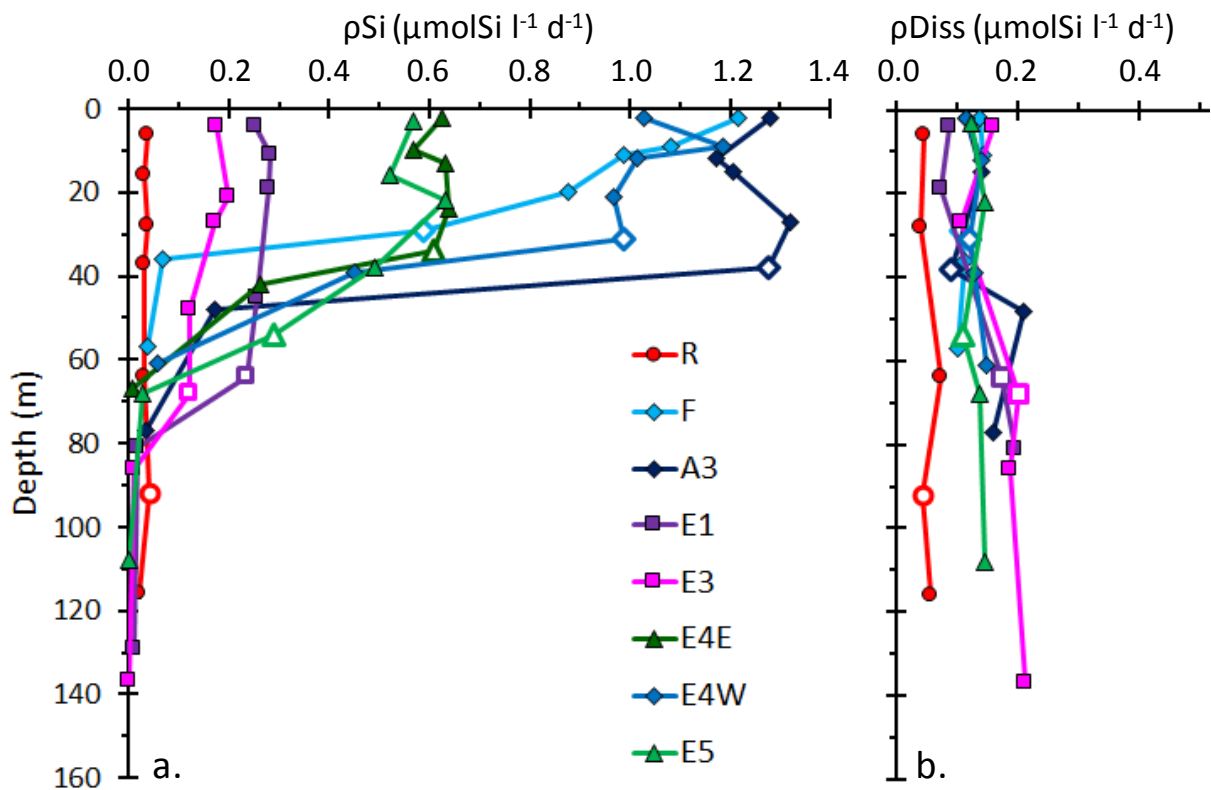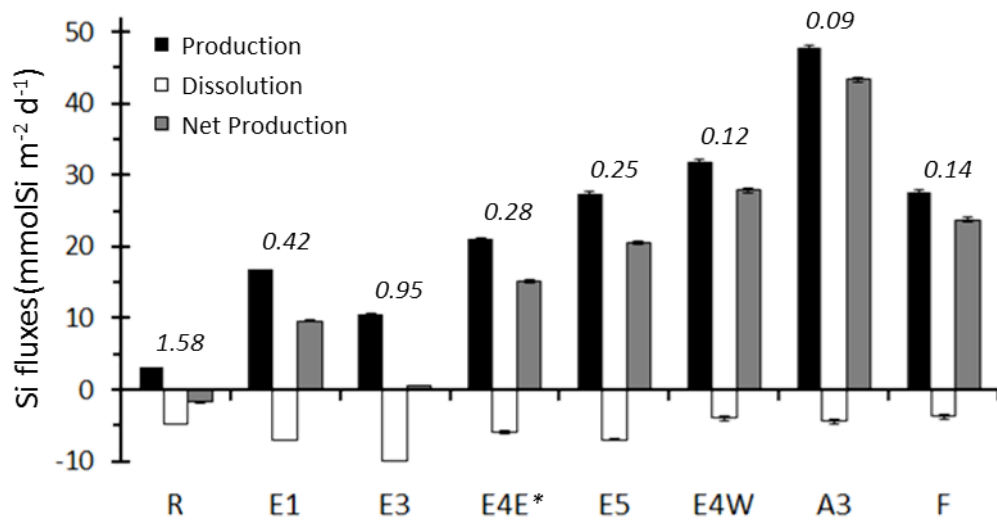
1172   * Since no dissolution rates were measured at E4E, dissolution and net production do not correspond to

1173   calculations from direct measurements but only to estimations. Dissolution was calculated as the average of all
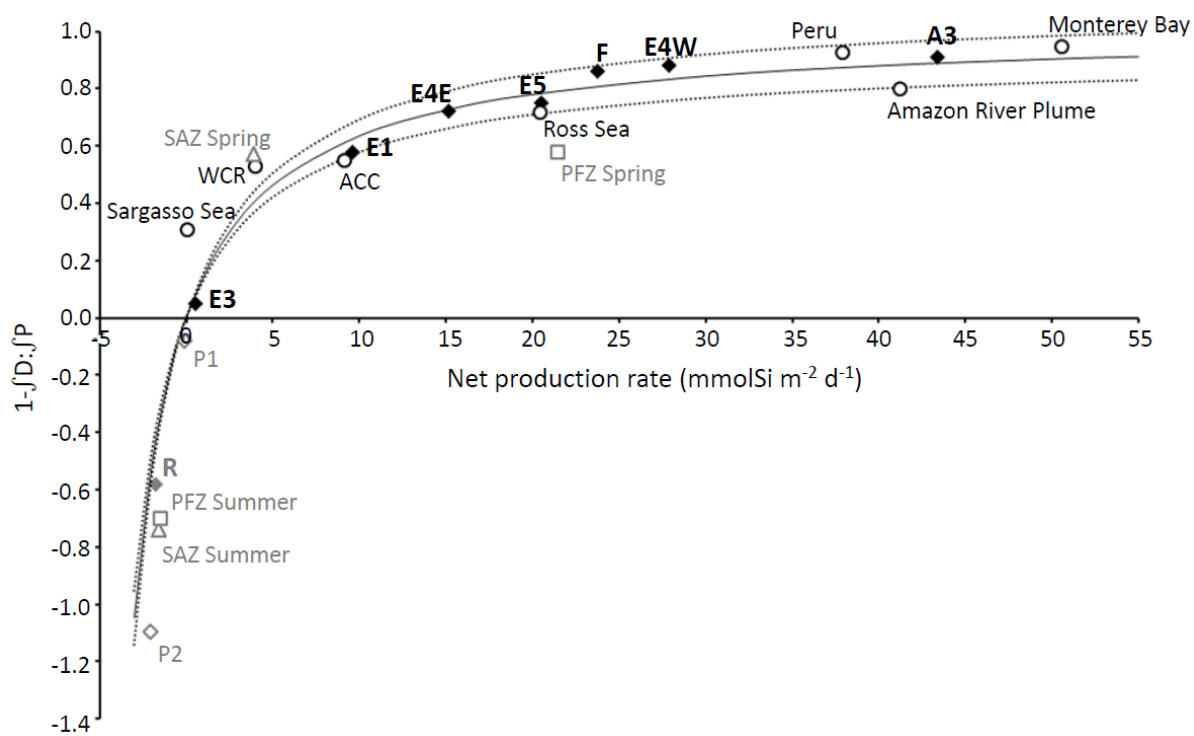
1174   KEOPS-2 integrated dissolution rates.
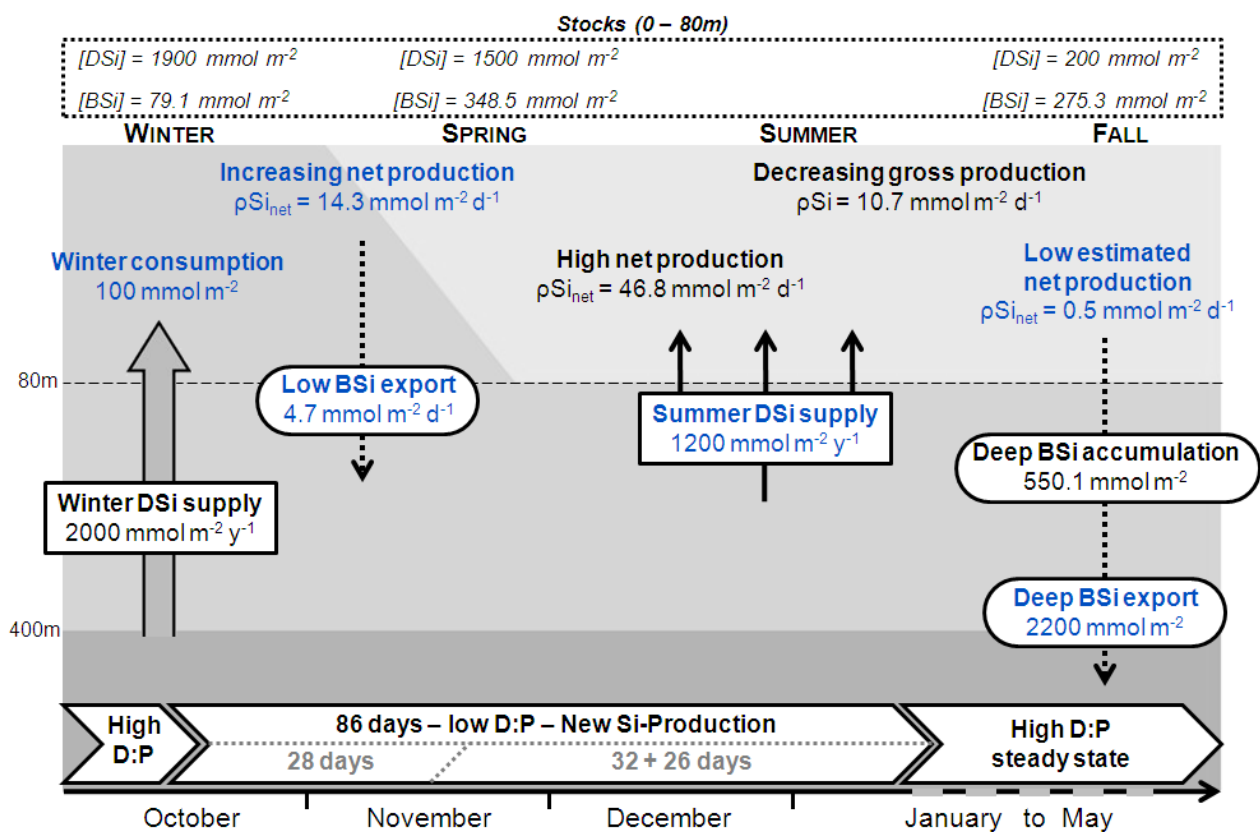
1175   Figure 5.

1176

1177   Figure 6.

1178

1179   Figure 7.